Physics – Uspekhi **55** (7) 639 – 656 (2012)

REVIEWS OF TOPICAL PROBLEMS

PACS numbers: 74.25.Uv, 74.25.Wx, **74.72.–h**

Dynamical magnetic structures in superconductors and ferromagnets

L S Uspenskaya, A L Rakhmanov

DOI: 10.3367/UFNe.0182.201207a.0681

Contents

Abstract. **The mixed state of type-II superconductors exhibits various types of instability (such as the dendrite instability, macroturbulence, chains of macroscopic flux droplets, and twister nucleation), resulting in macroscopic-scale spatial magnetic structures. Analysis reveals a certain analogy between remagnetization dynamics in superconductors and ferromagnets, thus allowing a deeper insight into the subject.**

1. Introduction

The formation of spatial structures is a quite general property of complex physical systems. The competition of contributions of various natures to the free energy frequently leads to a situation where an inhomogeneous state is thermodynamically more favorable than a homogeneous one. In particular, the formation of spatially inhomogeneous magnetic structures is characteristic of the majority of magnetically active media. To exemplify, we can mention domains in ferromagnets or intermediate states in type-I superconductors. The spatial scale of inhomogeneous magnetization can vary in a wide range, from a few lattice parameters (e.g., in the case of electron-induced phase separation in manganites) to the dimensions of macroscopic samples (e.g., in the case of magnetic domains in ferromagnets). Macroscopic magnetic structures containing a large number of Abrikosov vortices are also observed in type-II superconductors (in both high-temperature and traditional low-temperature superconductors). The vortices interact with one another and also with the sample boundaries and defects. Stray magnetic fields appear around samples with a demagnetizing factor. All these effects favor the appearance of inhomogeneous magnetic structures in superconductors, similarly to how analogous mechanisms lead to the formation of domains in ferromagnets.

The magnetic structures can move, change their shape and scale, and transform the sample from one magnetic phase into another. Such dynamic effects can occur spontaneously or due to changes in the temperature, magnetic field, or mechanical stresses. An important role in the dynamics of magnetic structures belongs to dissipative processes, which can control not only the relaxation but, frequently, also the topology of the inhomogeneous state in ferromagnets and superconductors. The macroscopic dynamic effects in superconductors and ferromagnets are an important class of physical phenomena observed in these systems. Their study is of great importance from the standpoint of both physics and various applications. In this review, we present a rather full description of macroscopic dynamic effects in superconductors, and in the last section, we draw an analogy between the classes of such phenomena in superconductors and ferromagnets.

One of the most fruitful approaches to studying macroscopic magnetic structures is the use of direct visualization methods, such as magnetic decoration and magnetooptical imaging. In this review, we frequently use results of magnetooptical (MO) studies.

The vortex structures in type-II superconductors can manifest instabilities of various natures. The best known of them is the thermomagnetic instability, or magnetic-flux jumps, which were revealed half a century ago. We note that precisely magnetic-flux jumps restrict the current-carrying capacity of commercial superconductors. Therefore, the nature of the flux jumps, the criteria of their appearance, and the methods for controlling them have been studied in numerous experimental and theoretical works. But only the use of high-resolution magnetooptics permitted revealing other types of macroscopic dynamic phenomena in type-II superconductors in the mixed state. It has been discovered

L S Uspenskaya Institute of Solid State Physics,
Russian Academy of Sciences,
ul. Ossipyana 2, 142432 Chernogolovka, Moscow region,
Russian Federation
Tel. +7 (496) 522 82 08. E-mail: uspenska@issp.ac.ru
A L Rakhmanov Institute for Theoretical and Applied Electromagnetics,
Russian Academy of Sciences,
ul. Izhorskaya 13, 125412 Moscow, Russian Federation
E-mail: alrakhmanov@mail.ru

Received 29 August 2011, revised 13 September 2011
Uspekhi Fizicheskikh Nauk **182** (7) 681 – 699 (2012)
DOI: 10.3367/UFNr.0182.201207a.0681
Translated by S N Gorin; edited by A M Semikhatov

that under certain conditions, the thermomagnetic instability is developed spatially inhomogeneously. The vortex lines move with a very high velocity inside the spontaneously forming channels — dendrites. As a result, the magnetic flux in a superconductor forms a complex fractal structure. Magnetooptical observations made it possible to reveal the macroturbulent instability in single crystals of high-T_c superconductors (HTSCs) and a number of other phenomena that are described in this review. It has also been found that almost all these dynamic effects have analogs in the physics of ferromagnetic domains.

2. Methods for studying magnetic structures

In this section, we briefly consider methods for visualizing magnetic structures. These methods can be divided into the following groups: (1) observation of the distribution of stray fields on the surface of an object under investigation and the restoration of the distribution of induction in the sample; (2) observation of the effect of local magnetization on the polarization of transmitted or reflected beams (of light, electrons, etc.) and the restoration of the distribution of induction from the changes in the polarization; (3) observation of lattice distortions caused by the presence of local magnetization and the restoration of the magnetic domain structure.

The first group includes the powder-figure method (Bitter technique) [1] and high-resolution decoration [2–4], scanning probe microscopy [5–11] and scanning of the surface using Hall probes [12, 13] or measurements of the induction distribution using lattices of Hall probes [14], and magneto-optical visualization using indicator films deposited [15, 16] or applied onto the surface [17–21].

The second group includes magnetooptical methods of observation of magnetic domains based on the dependence of optical constants on the direction and magnitude of magnetization in the medium: the birefringence of polarized light (Cotton–Mouton effect) [22–24], the rotation of the plane of polarization of light upon the transmission of light through a magnetically active medium (Faraday effect) [25–29], and the rotation of the plane of polarization of light upon reflection (Kerr effect) [30–32], as well as Lorentz microscopy [33] and diffraction of spin-polarized neutrons [34–39].

And, finally, owing to magnetoelastic distortions, the magnetic domain structure can be restored from X-ray-topography patterns [40, 41].

Among the above methods, precisely the magnetooptical methods of visualization [15–32] prove to be most suitable for studying the kinetics of magnetization reversal and of dynamic configurations of magnetic fluxes, because they allow observing both local (with a resolution not worse than $\lambda/2$) and macroscopic distributions of magnetization with the magnetic field sensitivity reaching 1 Oe. In addition, they exhibit a high time resolution, limited only by the duration of the illuminating pulse (about 10 ns).

3. Dynamic effects in type-II superconductors

3.1 Magnetic-flux jumps

Magnetic-flux jumps, or thermomagnetic instabilities, were historically the first macroscopic dynamic process that was revealed in type-II superconductors. The nature of this instability is related to the positive feedback between the electromagnetic and thermal processes in superconductors. The density of the superconducting current, which shields the external magnetic field, decreases with increasing the temperature. If a local region of heating arises in the superconductor for some reason, this leads to a decrease in the local current density. Because of the decrease in the shielding current, the magnetic flux penetrates deeper into the superconductor. The motion of the magnetic flux induces an electric field and, consequently, the appearance of additional Joule heat, i.e., further heating, and so on. Under certain conditions, such a process takes an avalanche-like character, leading to the transition of a part of the sample (or even of the entire sample) to the normal state. A detailed description of the theoretical and experimental studies of magnetic-flux jumps can be found in reviews [42, 43]. Here, we only briefly dwell on the basic aspects of the theory of this phenomenon.

The commonly accepted theory of thermomagnetic instability predicts that magnetic-flux jumps are developed more or less homogeneously, occupying a significant part of the sample volume, the front of the propagating magnetic flux remains smooth, and its shape depends on the shape of the sample surface and the shape of the region affected by the 'bare' (external) perturbation, which is transformed into a flux jump. In other words, the spatial scale of the most 'dangerous' instability is limited only by the size of the sample, and small-scale perturbations are stabilized due to heat conductivity and external cooling.

We consider the problem with simple geometry (Fig. 1). Let the plate of a type-II superconductor be placed in an external magnetic field $\mathbf{H}$ directed along the z axis. The external field is shielded by the current flowing along the y axis and the magnetic induction $\mathbf{B}(x)$ decreases in moving further into the sample. The density of the shielding current is determined by the current–voltage curve (CVC) of the superconductor, which is written as

$$\mathbf{j} = j_s(T, E)\,\frac{\mathbf{E}}{E}\,. \tag{1}$$

Here, for simplicity, we neglect the dependence of the density of the superconducting current j_s on the magnetic field, because it is known [42, 43] that taking it into account is unimportant for the description of the physics of thermomagnetic instability. The distribution of the magnetic field in the sample is described by a Maxwell equation with a boundary condition:

$$\operatorname{rot}\mathbf{B} = \mu_0\,\mathbf{j}\,, \qquad \mathbf{B}\big|_{x=0} = \mu_0\mathbf{H}\,, \tag{2}$$

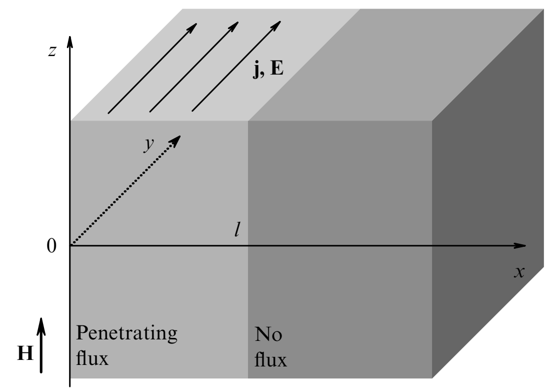

Figure 1. Geometry of the problem.

which is valid if the field H is mush greater than the first critical field H_{c1}. The temperature of the sample is determined from the heat conductance equation

$$C\,\frac{\partial T}{\partial t} = \kappa\Delta T + \mathbf{j}\,\mathbf{E}\,, \tag{3}$$

where C and κ are respectively the heat capacity and heat conductivity, and the electric field is found from the Maxwell equation

$$\mathrm{rot}\,\mathbf{E} = -\frac{\partial \mathbf{B}}{\partial t}\,. \tag{4}$$

The last two equations should be supplemented by appropriate boundary conditions. We eliminate the magnetic induction from the set of equations; instead of Eqns (2) and (4), we then write

$$\mathrm{rot}\,\mathrm{rot}\,\mathbf{E} = -\mu_0\,\frac{\partial \mathbf{j}}{\partial t}\,. \tag{5}$$

We assume that in the above geometry, all the quantities depend only on the coordinate x and that the initial state of the system is stationary, i.e., the temperature $T = T_0(x)$ and the field $E = E_0(x)$ are independent of time. Let a weak perturbation appear in the system:

$$T = T_0(x) + \delta T(x,t)\,, \qquad E = E_0(x) + \delta E(x,t)\,. \tag{6}$$

We assume for simplicity that the initial electric field E_0 is small and neglect this field. Then, substituting (6) in Eqns (3) and (5), in the approximation linear in the perturbations, we obtain

$$\begin{aligned} &C\,\frac{\partial\delta T}{\partial t} = \kappa\,\frac{\partial^2\delta T}{\partial x^2} + j_s\,\delta E\,,\\ &\frac{\partial^2\delta E}{\partial x^2} = \mu_0\left(\frac{\partial j_s}{\partial E}\,\frac{\partial\delta E}{\partial t} + \frac{\partial j_s}{\partial T}\,\frac{\partial\delta T}{\partial t}\right). \end{aligned} \tag{7}$$

Following the standard procedure of the stability analysis of equations, we seek their solutions in the form

$$\begin{aligned} &\delta T(x,t) = \delta T\exp\left(\mathrm{i}kx + \lambda t\right),\\ &\delta E(x,t) = \delta E\exp\left(\mathrm{i}kx + \lambda t\right). \end{aligned} \tag{8}$$

Substituting these expressions in the first equation in (7), we obtain the relation between the temperature and electric field perturbations: $\delta E = (\lambda C + k^2\kappa)\,\delta T/j_s$. Using this relation and formulas (8), from the second equation (7), we obtain a quadratic equation for the instability-growth increment λ,

$$\mu_0\,\frac{\partial j_s}{\partial E}\,\lambda^2 + \left(\mu_0\,\frac{j_s}{C}\,\frac{\partial j_s}{\partial T} + \mu_0\,\frac{\partial j_s}{\partial E}\,k^2\,\frac{\kappa}{C} + k^2\right)\lambda + k^4\,\frac{\kappa}{C} = 0\,. \tag{9}$$

The flux jump is developed if perturbations growing in time exist, i.e., Eqn (9) has solutions with $\mathrm{Re}\,(\lambda) > 0$. Because the differential conductivity of the superconductor in a small electric field is always positive ($\sigma(E) = \partial j_s/\partial E > 0$), the sign of the real part of the root of Eqn (9) is determined by the sign of the coefficient at the first power of λ. Hence, $\mathrm{Re}\,(\lambda) > 0$ if

$$\mu_0\,\frac{j_s}{Ck^2}\left|\frac{\partial j_s}{\partial T}\right| > \mu_0\sigma(E)\,\frac{\kappa}{C} + 1\,, \tag{10}$$

where we took into account that the current density in the superconductor decreases with temperature ($\partial j_s/\partial T < 0$).

According to criterion (10), large-scale perturbations of the largest possible size $l \sim 1/k$ are the most dangerous for stability. In the chosen geometry, such a size is the thickness of the region through which the shielding current flows, i.e., $l = H/j_s$. Condition (10) can then be rewritten as

$$\mu_0\,\frac{H^2}{Cj_s}\left|\frac{\partial j_s}{\partial T}\right| > \mu_0\sigma(E)\,\frac{\kappa}{C} + 1\,. \tag{11}$$

Usually, $j_s/|\partial j_s/\partial T| \sim T_c$. The left-hand side of stability criterion (11) contains the ratio of the characteristic magnetic energy $\mu_0 H^2$ to the characteristic thermal energy CT_c. The right-hand side of the stability criterion includes two terms that are responsible for two stabilization mechanisms. The first includes the heat conductivity and differential conductivity. It is obvious that the greater the heat conductivity is, the more efficient the process of heat removal from the heated region and the more stable the superconducting state.

The role of differential conductivity can be understood equally easily. The density of the superconducting current decreases with heating, and the magnetic flux moves and leads to the appearance of an electric field. An increase in the electric field leads to an increase in the current density ($\partial j_s/\partial E > 0$), which in turn partly compensates the decrease in the current caused by heating. This is the so-called dynamic stabilization mode. If the first term is small compared to unity, a second (adiabatic) stabilization mechanism intervenes. If the ratio of the characteristic magnetic energy $\sim \mu_0 H^2$ to the characteristic thermal energy $\sim CT_c$ is small, no flux jumps arise.

Using Eqn (9), it can easily be found that near the instability threshold, the imaginary part of the increment λ is nonzero. This implies the possibility of the appearance of strong temperature and electric field fluctuations before the appearance of a flux jump, and a nonmonotonic character of the development of perturbations upon the appearance of instability.

The above theory and its more complex variants allow describing experimentally observed effects in the development of magnetic-flux jumps in superconductors of various types [43, 44].

3.2 Dendritic instability

The above-described picture of the development of thermomagnetic instability correctly describes many experimental facts, but by no means all of them. Numerous magnetooptical experiments show that the thermomagnetic instability can lead to the appearance of a branching (dendritic) structure of the magnetic-flux distribution [45–54]. Such a phenomenon develops especially frequently in thin films placed in a transverse magnetic field. The dendritic instability develops as follows (Fig. 2). As the external field increases, the magnetic flux penetrates inside the sample. In small fields, the front of this magnetic flux is smooth. Then, suddenly, fingerlike outbreaks of vortices into the bulk of the sample appear at the front (Fig. 2a), as if 'grass' starts to grow near the edge of the penetrating flux. Next, separate dendrites ('trees') start appearing in a stronger external field (Fig. 2b). With a further increase in the external field, the number of dendrites becomes greater and greater (Fig. 2c). Gradually, the entire sample becomes filled by the 'forest' of dendrites, and the distribution of the magnetic field takes a typical fractal form (Fig. 2d). The dendrites develop quite rapidly. When using the magnetooptical method for observation, an impression forms that the dendrite arises instantaneously.

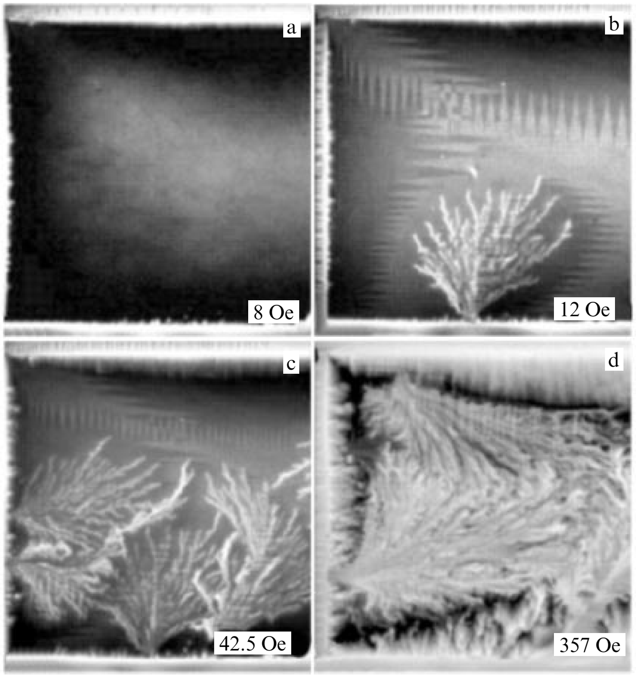

Figure 2. Magnetooptical images of the development of a dendritic instability in an NbN film at $T = 4$ K (the magnetic field is applied transversely to the film plane). The lighter regions correspond to a greater magnetic field strength. Only the left-hand side of the sample is shown; its length is 2.4 mm. In the right-hand corner of each image, the applied magnetic field strength is indicated [53].

Dendritic instability has been observed at temperatures below 10–15 K in films of low-temperature superconductors (Nb, Nb_3Sn, NbN), in films of magnesium diboride, in films and single crystals of HTSCs $YBa_2Cu_3O_7$, $BiSr_2CaCu_2O_8$, and in some other materials.

The above-described behavior seems to contradict the 'classical' concepts of the development of thermomagnetic instability. Indeed, because heat conductivity suppresses the development of such an instability, the small transverse size of a dendrite seems to favor the fast removal of heat from its channel. Consequently, a thermal fluctuation of a large spatial scale should develop faster than a narrow dendrite. But a detailed analysis of experimental data unambiguously indicates the thermal nature of the appearance of a dendritic structure (see [55] and the references therein). This follows from the direct measurements of temperature in dendrite channels using a thermal imager, the fact that such a structure arises only in the region of low temperatures, where the heat capacity of the material is small, and a detailed comparison of experiments with the results of the theory where a dendrite is treated as a consequence of local thermomagnetic instability [56, 57]. A dendritic spatial structure arises upon the development of a flux jump if the background electric field in a superconductor produced by an external regular source or by a random action exceeds some critical value E_c, which depends on the geometry of the sample. We note that because of the effect of the geometrical factor, the value E_c for films is less than for massive samples. Correspondingly, the development of the dendritic instability is more probable in films.

The physical reason for the development of a dendritic structure in superconductors can be understood from the following considerations. If a perturbed region extended in the direction transverse to the current vector appears in the sample, then the current cannot bypass this region and flows through it and heats it up. If the electric field E produced by an external source is sufficiently large ($E > E_c$), then the heating of the perturbed region exceeds the heat removal, leading to the development of a dendrite. The characteristic thickness of the dendrite $\Delta d \sim (\kappa/|E\,\partial j_s/\partial T|)^{1/2}$ is determined by the balance between the heating and the heat removal. In films, the rate of growth of a dendrite is determined by electromagnetic processes in the space surrounding the film and can reach giant magnitudes, 10^5 m s^{-1} and greater.

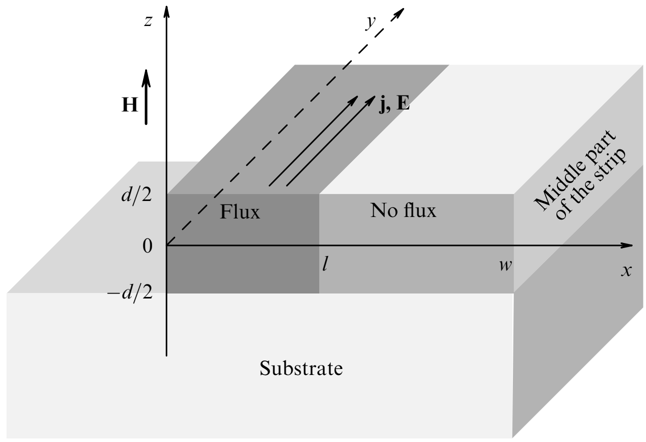

Figure 3. Film on a substrate (left-hand edge of the sample). The dark gray shading corresponds to the region into which the magnetic flux has penetrated.

Following [56], we find conditions under which a dendritic structure arises in a film. Let a film of thickness d and width $2w$ lie on a massive substrate and let the magnetic flux penetrate into the film to a depth l. The film is located in the xy plane and the magnetic field is applied perpendicularly to the film along the z axis (Fig. 3). For the analysis, we use CVC (1) of the superconductor, Maxwell equations (2), and heat conductance equation (3). As before, we neglect the dependence of the current density on the magnetic field. The concrete form of the function $j_s(E)$ is unimportant for us. It is only important that the CVC of the superconductor be very steep:

$$n(E) \equiv \frac{\partial \ln E}{\partial \ln j} \approx \frac{j_s}{\sigma(E)E} \gg 1\,. \tag{12}$$

The parameter $n(E)$ generalizes the power-law CVC ($E \propto j^n$), which is frequently used in approximating experimental data. The key dimensionless quantity in the theory is the ratio of the coefficients of thermal and magnetic diffusion:

$$\tau \equiv \frac{\mu_0 \kappa \sigma(E)}{C}\,. \tag{13}$$

The greater τ is, the more rapid the propagation of heat and the slower the motion of the magnetic flux. Consequently, the smaller τ is, the less stable the superconducting state and the more probable the formation of dendrites.

We assume that the film is thin and wide, $d \leqslant \lambda_L \ll \sqrt{dw}$, where λ_L is the London penetration depth. Then the magnetic flux penetrates into a long film to the depth [58–60]

$$l = \frac{\pi^2 w H^2}{2d^2 j_c^2}\,, \tag{14}$$

where H is the applied magnetic field. We assume that $\lambda_L \ll l \ll w$.

The solution of Eqns (2) and (3) is sought in the form of small perturbations on the background of the stationary state $(T, \mathbf{E}, \mathbf{j})$. We assume that the background temperature is uniform in the film and the electric field is homogeneous in the layer into which the magnetic flux has penetrated. The last assumption is, naturally, approximate. However, a numerical analysis shows that it leads to only small changes in the final results [56, 57]. For the current perturbation, using (1), we obtain,

$$\delta\mathbf{j} = \left(\frac{\partial j_s}{\partial T}\,\delta T + \sigma\,\delta E_y\right)\frac{\mathbf{E}}{E} + j_s\,\frac{\delta\mathbf{E}_x}{E}\,. \tag{15}$$

We seek perturbations over the stationary state in the form

$$\begin{aligned}
\delta T &= T^*\theta \exp\left(\frac{\lambda t}{t_0} + \mathrm{i}k_x\xi + \mathrm{i}k_y\eta\right),\\
\delta E_{x,y} &= E\,\varepsilon_{x,y}\exp\left(\frac{\lambda t}{t_0} + \mathrm{i}k_x\xi + \mathrm{i}k_y\eta\right),\\
\delta j_{x,y} &= j_s\,i_{x,y}\exp\left(\frac{\lambda t}{t_0} + \mathrm{i}k_x\xi + \mathrm{i}k_y\eta\right),
\end{aligned} \tag{16}$$

where θ, ε, and i are dimensionless quantities depending on z, $\xi = x/a$, $\eta = y/a$, $\zeta = z/a$, $a = \sqrt{CT^*/\mu_0 j_c^2}$, $T^* = -(\partial \ln j_s/\partial T)^{-1}$, and $t_0 = \mu_0\sigma a^2$. The existence of solutions with a positive real part of the eigenvalue λ means the existence of an instability. From Eqn (15), we then obtain

$$i_x = \varepsilon_x\,, \qquad i_y = \theta + n^{-1}\varepsilon_y\,, \tag{17}$$

and from Maxwell equation (2) and heat conductance equation (3), we obtain

$$\begin{aligned}
&\mathbf{k}\times[\mathbf{k}\boldsymbol{\varepsilon}] = \lambda n\,\mathbf{i}\,,\\
&\lambda\theta = \tau\left(-k_y^2\theta + \frac{\partial^2\theta}{\partial\zeta^2}\right) + (i_y + \varepsilon_y)\,n^{-1}\,.
\end{aligned} \tag{18}$$

Because we are interested in solutions of the dendritic form, for which $k_y \gg k_x$, we neglected the heat conductivity along the dendrite axis.

Because the film is thin, perturbations change only a little over its thickness. We integrate (17) over the film thickness, assuming that the temperature of the substrate is equal to T. We set $h_0 = -(\partial q_0/\partial T + \partial q_s/\partial T)$, where $q_s(T)$ and $q_0(T)$ are the respective heat fluxes into the substrate and into the cooler. After the integration of the second equation in (18), we then obtain

$$\theta = \frac{(1+n^{-1})\,\varepsilon_y}{n\lambda + n\tau(k_y^2 + h) + 1}\,, \tag{19}$$

where $h = 2h_0 a^2/\kappa d$. We seek solutions for the perturbations in the region into which the field has penetrated, $0 \leqslant \xi \leqslant l/a$. It is obvious that at the external face of the film, $\delta j_x = 0$ and hence $\delta E_x = 0$. In the Meissner state, all the perturbations are equal to zero, or $\delta E_x = \delta T = \delta j_y = 0$ at $\xi = l/a$. Then the boundary conditions for the electric field are satisfied only if $k_x = (\pi a/2l)(2s+1)$, $s = 0, 1, 2, \ldots$. Integrating the first equation in (18), we obtain

$$\begin{aligned}
&-\mathrm{i}k_y(k_x\varepsilon_y + \mathrm{i}k_y\varepsilon_x) - \frac{2a}{d}\,\varepsilon_x' = -\lambda n\varepsilon_x\,,\\
&-k_x(k_x\varepsilon_y + \mathrm{i}k_y\varepsilon_x) + \frac{2a}{d}\,\varepsilon_y' = -\lambda n f(\lambda, k_y)\,\varepsilon_y\,,
\end{aligned} \tag{20}$$

where

$$f(\lambda, k_y) \equiv \frac{i_y}{\varepsilon_y}\,\frac{1}{n} - \frac{1+n^{-1}}{n\lambda + n\tau(k_y^2 + h) + 1}\,.$$

Using the Biot–Savart equation, we obtain the perturbation of the magnetic field in a thin film $((d/a)^2 \ll 1)$ in the form

$$\begin{aligned}
&\delta B_{x,y} = \pm\mu_0\zeta d\int_0^{l/a}\mathrm{d}\xi'\int_{-\infty}^{\infty}\mathrm{d}\eta'\,G(\xi-\xi', \eta-\eta')\,\delta j_{y,x}\,,\\
&G(\xi,\eta) = \frac{1}{4\pi\left[\xi^2 + \eta^2 + (d/2a)^2\right]^{3/2}}\,,
\end{aligned} \tag{21}$$

where the integration is also performed over the region of the Meissner state, but because the function $G(\xi,\eta)$ decreases rapidly as its arguments increase, this contribution gives only insignificant numerical corrections. From the Maxwell equation, we obtain the following relation between the electric and magnetic field perturbations: $\delta E'_{x,y}/E = \mp\lambda n\delta B_{y,x}/\mu_0 a j_s$. After the Fourier transformation and algebraic calculations, system (20) can be represented as

$$\begin{aligned}
&-\mathrm{i}(k_x k_y\varepsilon_y + k_y^2 + \lambda n)\varepsilon_x = \frac{\lambda n d}{2a}\sum_{k_x'} G_x(k_x, k_x', k_y)\,\varepsilon_x(k_x')\,,\\
&(k_x^2 + \lambda n f)\varepsilon_y + \mathrm{i}k_x k_y\varepsilon_x = \frac{\lambda n f}{2a}\sum_{k_x'} G_y(k_x, k_x', k_y)\,\varepsilon_y(k_x')\,,
\end{aligned} \tag{22}$$

where

$$\begin{aligned}
&\begin{pmatrix} G_x(k_x, k_x', k_y)\\ G_y(k_x, k_x', k_y)\end{pmatrix} = 4\int_0^{l/a}\mathrm{d}\xi\int_0^{l/a}\mathrm{d}\xi'\,G(\xi-\xi', k_y)\\
&\qquad\times\begin{pmatrix}\sin(k_x\xi)\sin(k_x'\xi')\\ \cos(k_x\xi)\cos(k_x'\xi')\end{pmatrix},\\
&G(\xi, k_y) = \frac{k_y a}{2\pi l}\,\frac{K_1\left[k_y\sqrt{\xi^2 + (d/2a)^2}\right]}{\sqrt{\xi^2 + (d/2a)^2}}\,.
\end{aligned}$$

The result of the numerical calculation of the increment of the perturbation growth $\mathrm{Re}\,\lambda$ for a thin film ($\alpha = d/2l \ll 1$) is shown in Fig. 4.

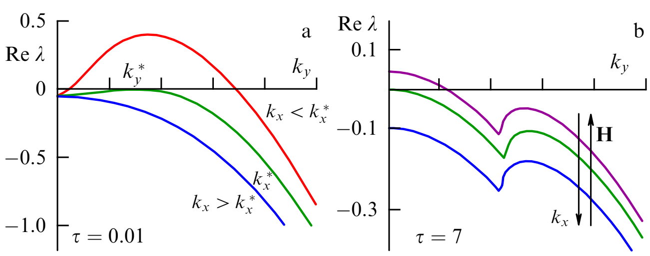

Figure 4. Results of a numerical solution of Eqns (22) for small (0.01) and large (7) values of the parameter τ, $\alpha = 0.001$, and $n = 20$ [56].

In the first approximation in $\alpha \ll 1$, we can also find an analytic equation for λ [56],

$$A_1\lambda^2 + A_2\lambda + A_3 = 0\,, \tag{23}$$

where

$$A_1 = n\gamma\alpha\,, \qquad A_2 = k_y^2(1+\tau A_1) + nk_x^2 + A_1(h\tau - 1)\,,$$

$$A_3 = k_y^4\tau + nk_x^2k_y^2\tau + nk_x^2\left(h\tau + \frac{1}{n}\right) + k_y^2(h\tau - 1)\,,$$

and γ is a slowly changing function of k_x, $\gamma \approx 5$.

If the instability develops homogeneously ($k_y = 0$), we find from (23) that $\mathrm{Re}\,\lambda > 0$ if

$$h\tau < 1 - \frac{k_x^2}{\gamma\alpha}\,. \tag{24}$$

If the external field is small, $l/w \ll 1$, then $k_x \propto 1/l$ is large and the system is stable. As the field increases, an instability can occur. However, the instability develops only if the heat removal from the film is small, $h\tau < 1$. If $h\tau \ll 1$ (adiabatic conditions), then the instability appears if $k_x^2/\gamma\alpha < 1$, or, in dimensional notation, $\mu_0 j_c^2 ld > CT^*(\pi^2/2\gamma)$. Assuming that the field penetrates into the film over a small depth, $l \ll w$, we can use (14) to rewrite the last inequality in the form $H > H_{\mathrm{ad}}$, where

$$H_{\mathrm{ad}} = \sqrt{\frac{d}{w}\,\frac{CT^*}{\gamma\mu_0}} \sim \sqrt{\frac{d}{w}}\,H_{\mathrm{ad}}^{\mathrm{sl}} \tag{25}$$

and $H_{\mathrm{ad}}^{\mathrm{sl}}$ is the field corresponding to the development of the instability in a massive plate (slab) in the field that is parallel to its surface under adiabatic conditions.

From the results of numerical calculations of Eqns (22) for $\tau \ll 1$ shown in Fig. 4a, it follows that in small fields ($k_x > k_x^*$), the film is stable at any k_y. In higher fields ($k_x < k_x^*$), the instability arises in a certain range of k_y. Consequently, perturbations with a certain spatial structure begin to grow. They have the form of 'fingers,' with enhanced temperature and electric field, extended perpendicularly to the front of the penetrating magnetic flux. This is the beginning stage of the development of the dendritic instability. If $\tau \gg 1$ (Fig. 4b), the instability develops homogeneously because thermal processes dominate the electrodynamic ones.

We estimate the critical values of k_y^* and k_x^* (see Fig. 4) at which the instability development begins. The value of k_x^* determines the magnetic field corresponding to the instability; k_y^* determines the transverse size of the dendrites. The equation for k_y^* and k_x^* has the form $\max\{\mathrm{Re}\,\lambda\} = 0$. In the limit $\alpha \ll 1$ in (23), it can be assumed that $A_1 = 0$. Then

$$\lambda = (k_y^2 + h)\tau + \frac{k_y^2 - k_x^2}{k_y^2 + nk_x^2}\,. \tag{26}$$

Hence,

$$k_x^* = \frac{\sqrt{n+1} - \sqrt{nh\tau}}{n\sqrt{\tau}}\,, \qquad k_y^* = \frac{\left[\sqrt{nh\tau+1}\,\left(\sqrt{n+1} - \sqrt{nh\tau+1}\,\right)\right]^{1/2}}{\sqrt{n\tau}}\,. \tag{27}$$

Because we always have $n \gg 1$ in the case of superconductors, it follows from the above relations that $k_y^*/k_x^* \geqslant n^{1/2} \gg 1$ if $h\tau < 1$. The inequality $k_y^* \gg k_x^*$ means that upon the development of the instability, a longitudinal structure of the penetrating magnetic flux arises, i.e., 'fingers' appear that are extended along the normal to the sample faces.

At a sufficiently large value of τ, the instability develops homogeneously. The critical value τ_c that corresponds to the transition from the dendritic instability to a homogeneous development of a magnetic flux jump can be found from the condition $\mathrm{Re}\,\lambda(k_x = k_x^*, k_y = 0) = 0$. In this case, $\tau_c = (1 - k_x^{*2}/\gamma\alpha)/h$. Substituting k_x^* and α in the last relation, we obtain

$$\sqrt{n\tau_c}\,\left(1 + \sqrt{h\tau_c}\,\right) = \frac{\pi a}{\gamma d}\,. \tag{28}$$

Using Eqn (28) and the above formulas, we find that if the external heat removal h_0 is large ($h_0 > h_c$), then the instability is developed only in the form of dendrites. The parameter h_0 is defined in the text after Eqn (18) and

$$h_c = \frac{2\gamma^2\mu_0^2 j_c^4 d^3 \kappa n}{\pi^2 T^{*2} C^2}\,. \tag{29}$$

If $h_0 < h_c$, then, depending on the conditions, either a homogeneous flux jump or a dendritic instability can arise.

It follows from Eqns (12) and (13) that $E \approx j_s\mu_0\kappa/nC\tau$. Using this relation and Eqn (28), we can construct a stability diagram on the plane (E, H) for different values of h_0 (Fig. 5). The thermomagnetic instability develops as a uniform jump of the magnetic flux if $H > H_{\mathrm{uni}}(h_0, E)$. The dendrites arise if $H > H_{\mathrm{fing}}(h_0, E)$.

Using Eqns (14), (24), and (25), we obtain

$$H_{\mathrm{uni}} = H_{\mathrm{ad}}\left(1 - \frac{2T^*h_0}{ndj_sE}\right)^{1/2}. \tag{30}$$

At $h\tau \ll 1$ and $n \gg 1$, it can be easily found that

$$H_{\mathrm{fing}} = \left(\frac{j_s d^2}{\pi w}\sqrt{\frac{\kappa T^* j_s}{E}}\right)^{1/2}. \tag{31}$$

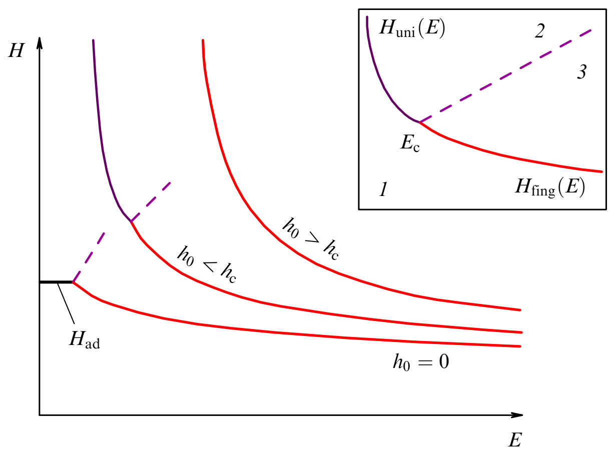

Figure 5. Stability diagram on the (E, H) plane at various values of the heat removal coefficient h_0. At a given h_0, the instability arises in fields lying above the corresponding curve $H(E)$. To the left of the dashed line, the instability develops uniformly; to the right, in the form of dendrites. The inset schematically shows the diagram on a larger scale: region *1* corresponds to a stable state; *2*, to a homogeneously instable state; and *3*, to a dendritic instability [56].

If $h_0 \leqslant h_c$, then the curves $H_{\text{fing}}(E)$ and $H_{\text{uni}}(E)$ intersect at $E = E_c(h_0)$. If $h_0 \geqslant h_c$, then $H_{\text{fing}}(E) < H_{\text{uni}}(E)$ at any E and only the dendritic instability is possible.

We see that the dendritic instability develops in superconductors that are in good thermal contact with the external medium (substrate or cooler) if the electric field induced in the superconductor by external perturbations is sufficiently large. The observation of dendrites in films is more probable than in massive single crystals. At the parameters values characteristic of low (helium) temperatures ($j_s = 10^{10}$ A m^{-2}, $C = 10^3$ J K^{-1} m^{-3}, $\kappa = 10^{-2}$ W K^{-1} m^{-1}, $T^* = 10$ K, and $d = 0.3$ μm), we obtain $E_c \approx 4 \times 10^{-4}$ V m^{-1}. Similar estimates for the electric field E_c in the case of a massive sample yield $E_c^{\text{sl}} \approx 0.1$ V m^{-1} [57]. The magnetic field for the development of the dendritic instability is much lower for a film than for a massive sample [56, 57]. Such a large difference in the conditions corresponding to the instability development in a film and in a massive sample is primarily due to the effect of stray magnetic fields on the dynamics of the magnetic flux. Numerical estimates show that the field corresponding to the development of the dendritic instability in thin films ranges from ten to several tens of oersteds, which is indeed observed in experiments.

The linear analysis describes only the initial stage of the dendritic instability development. It predicts that a periodic 'fingerlike' structure elongated in the direction perpendicular to the front of the penetrating magnetic flux arises first (Fig. 2a). The period of this structure can be estimated as follows. At $E = E_c$, $h\tau \ll 1$, and $n \gg 1$, we have

$$d_y = \frac{\pi^2 C T^*}{2\gamma n^{1/4} \mu_0 j_c^2 d}\,, \tag{32}$$

which for the characteristic values of the parameters and $n = 30$ yields $d_y \sim 100$ μm. A numerical simulation shows that as the field increases, one finger first begins growing, developing into a branching ('treelike') structure. Then the next dendrite starts growing. The lateral branches at the 'fingers' arise for the same physical reasons for which 'grass' appears near the film face. The structure observed in experiment has the transverse size about 20–50 μm, which agrees well with analytic estimates and numerical calculations. A thermomagnetic instability, both homogeneous and dendritic, can develop only in the region of low temperatures, because the parameter $\tau \sim C(T) \sim T^3$ rapidly increases with temperature and the quantity $h\tau$ becomes greater than unity. In experiment, instabilities in films are indeed observed at temperatures no higher than 10–15 K.

To estimate the conductivity in the regime of the flowing flux, we take $\sigma = 10^9$ Ω^{-1} m^{-1}; the characteristic time of the instability development is then $t_0 \approx 0.1$ μs. Because the characteristic length of a dendrite is about several millimeters, the dendrite propagation speed is 10–100 km s^{-1}. This estimate is confirmed by numerical calculations and by a more detailed analysis of the penetration of the magnetic flux into the Meissner phase. In an experiment with a moderate time resolution, it seems that the dendrites arise instantaneously. The flux penetration occurs at a high speed because magnetic field lines are strongly curved near the film surface and produce an additional tension force, which pushes the vortices into the sample. In the case of a massive sample, the time of the instability development is much higher.

3.3 Macroturbulence

Macroturbulence is one of the most interesting effects that have been revealed in studying the dynamics of magnetic fluxes in HTSCs using magnetooptical observations [61, 62]. This effect is observed in $YBa_2Cu_3O_x$ and in other $1-2-3$ HTSC systems in an alternating magnetic field, when vortices with an oppositely directed magnetic fluxes (vortices and antivortices) appear in the sample. Upon the development of the instability, a turbulent motion of the magnetic flux near the interface between the vortices and antivortices arises (Fig. 6).

Let a magnetic flux be trapped in a superconductor placed in an external magnetic field. Let then the external field change sign. The boundary corresponding to the zero magnetic induction separates regions containing vortices and antivortices (see Fig. 6). Below, for definiteness, we call that part of the Abrikosov vortices that were initially trapped in the superconductor 'vortices,' and those that entered into the sample after the external field changed sign 'antivortices.' In some range of temperatures and magnetic fields, such a distribution of the magnetic flux becomes unstable. Near the zero-induction line, the motion of the magnetic flux becomes chaotic, resembling turbulence in a conventional liquid. As this process develops, it is accompanied by the formation of fingers through which the antivortices penetrate into the region of vortices. As a result, the front of the magnetization reversal, at which the annihilation of vortices and antivortices occurs, takes an intricate shape, and its length increases. The annihilation process accelerates and is frequently terminated by the complete disappearance of vortices of one sense. The characteristic time of the instability development varies from tenths of a second to tens of minutes; the arising spatial structures contain a large number of vortices. Unfortunately, the available photos do not correctly represent the macroturbulence. In dynamics, it surprisingly resembles the turbulence in a conventional liquid.

Attempts to explain macroturbulence in terms of the thermal instability (by analogy with dendrites) have failed. The temporal and spatial scales of the process differ dramatically (by orders of magnitude) from the characteristic thermal scales and times. The thermal mechanism is also inconsistent with the fact that the macroturbulence develops

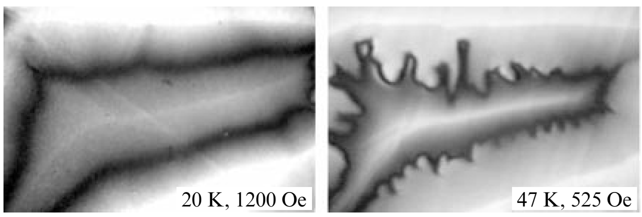

Figure 6. Patterns of the magnetic flux penetration into a single-crystal plate of $YBa_2Cu_3O_7$ cooled in a magnetic field. The dark lines correspond to the lines of zero induction that separate flux and antiflux regions. At the lower temperature, the flux–antiflux front is smooth and its shape remains unaltered in time (as an example, an image is given that corresponds to the applied field $H = 1200$ Oe at $T = 20$ K). At a higher temperature, a macroturbulence instability develops at the magnetization-reversal front: the vortices and antivortices accumulate near the front (the induction distribution across the front becomes an inhomogeneous function of the coordinate [63]); the originally relatively even front of the flux bends; at the bends, macroscopic droplets of vortices and antivortices are formed, which jumpwise break the front and annihilate (the image is obtained at $H = 525$ Oe and $T = 47$ K; courtesy of V K Vlasko-Vlasov, 1993).

at relatively high temperatures (no lower than 15–20 K) and manifests itself most strongly at $T = 40$–60 K. Taking the contribution of the annihilation of vortices and antivortices to dissipation into account [64] adds nothing, because this contribution is quite small [65]. The authors of [66] supposed that the process of the annihilation of vortices can be accompanied by the formation of a spatial region free from vortices (the so-called Meissner hole). The existence of such a region can cause an instability of the vortex distribution because of the induction of high-density currents that should flow around such a Meissner hole. However, the authors of [66] did not attempt to describe the development of macroturbulence in the framework of their hypothesis.

To construct a proper theory of macroturbulence, two factors must be taken into account. First, this instability arises only if vortices of different signs exist in the sample. Second, this instability is observed only in $1-2-3$-type HTSCs, which are characterized by a noticeable anisotropy in the crystallographic planes *ab* (the turbulence arises during motion in these planes). This anisotropy is especially strong in crystals with twins, because these are centers of pinning for the vortices moving transversely to the twins and are channels for the motion of vortices along the twins [67, 68]. But even in detwinned $1-2-3$ single crystals, the anisotropy of the critical current in the *ab* plane reaches 1.5–2.0.

Because of the anisotropy, the vortices move at an angle to the direction of the Lorentz force. As a result, the vortices and antivortices also move at an angle to the front of the magnetization reversal. Then the tangential velocity of the flux of vortices at this boundary undergoes a discontinuity. According to the classic Helmholtz theory [71], a stationary hydrodynamic flux under such conditions becomes unstable, and turbulence arises. This is why the temperature range in which macroturbulence is observed is wider in samples with a higher density of twins [72], and macroturbulence is absent in those regions of the crystal where the vortices move perpendicularly to the magnetization-reversal front [73]. We see in what follows that even a small anisotropy can lead to the appearance of macroturbulence.

Macroturbulence is usually observed in single-crystal plates placed in a magnetic field perpendicular to the *ab* plane. The penetration of the magnetic flux into a superconductor has its specificity [74]. But macroturbulence is also observed in crystals with a small demagnetizing factor [66, 69]. Therefore, for the description of the physics of the instability, we consider a sample of a simple geometry: a semi-infinite plate of thickness $2d$ in a magnetic field H that is parallel to the sample surface and is directed along the z axis, with the x axis perpendicular to the plate and the origin placed at the center of the sample (Fig. 7). The magnetic field first increases to a certain value much greater than H_{c1}, then decreases, changes sign, and reaches some negative value, which in the absolute value is also much greater than H_{c1}. As a result, two groups of vortices of different signs appear in the bulk, vortices located closer to the sample center and vortices at the periphery.

The vortices and antivortices are pinned on defects. They begin moving owing to the Lorentz force and the thermo-activational creep of the magnetic flux. There is also one more reason for the motion of vortices. The vortices and anti-vortices annihilate at the line of zero induction, which leads to a decrease in the number of vortices in the sample and to an increase in the number of antivortices, which continue penetrating into the volume from the boundary of the plate.

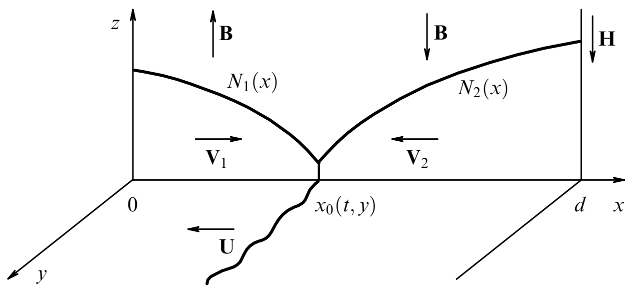

Figure 7. Magnetic flux distribution in a half-plate ($0 < x < d$). Vortices with a density $N_1(x)$ are located in the center of the plate; antivortices with a density $N_2(x)$ are located at the periphery.

As a result, the magnetization-reversal front moves with time to the center of the sample. We describe the motion of vortices in terms of the hydrodynamic approach, assuming that all spatial scales of the problem are much greater than the lattice parameter d_f of the lattice of vortices.

The densities of the vortices $N_1(x,y)$ and antivortices $N_2(x,y)$ are related to the magnetic induction $B(x,y)$ as $N_\alpha(x,y) = s_\alpha B(x,y)/\Phi_0$, $\alpha = 1,2$, where $s_1 = 1$, $s_2 = -1$, and Φ_0 is the magnetic flux quantum. The densities $N_\alpha(x,y)$ must satisfy the continuity equations

$$\frac{\partial N_\alpha}{\partial t} + \operatorname{div}(N_\alpha \mathbf{V}_\alpha) = 0\,, \tag{33}$$

where $\mathbf{V}_\alpha(x,y)$ are the hydrodynamic velocities of the vortices and antivortices. The electric field is determined by the Faraday law (following the original works, the calculations in this section are performed in the CGSE system):

$$\mathbf{E} = -\frac{1}{c}\,[\mathbf{VB}]\,. \tag{34}$$

From Eqns (33) and (34), we obtain

$$E_x = \frac{N_\alpha s_\alpha \Phi_0}{c}\,V_{\alpha y}\,, \qquad E_y = \frac{N_\alpha s_\alpha \Phi_0}{c}\,V_{\alpha x}\,. \tag{35}$$

The calculations can be performed in the general form, but to avoid too cumbersome formulas, we use a power-law model CVC:

$$J_X = \frac{1}{\varepsilon}\,J_s\left(\frac{E_X}{E_0}\right)^{1/m}, \qquad J_Y = J_s\left(\frac{E_Y}{E_0}\right)^{1/m}. \tag{36}$$

Here, X and Y are the anisotropy axes in the plane of motion of the vortices, the exponent (with $m > 1$) is the same for both directions, and $\varepsilon < 1$ is the anisotropy parameter of the CVC. For simplicity, we also assume that the X and Y axes are tilted at 45° to the crystal faces, as in the case in the majority of experiments. From Eqns (36), using equalities (35) and the Maxwell equation $[\nabla\mathbf{B}] = 4\pi\mathbf{J}/c$, we obtain the equations

$$\begin{aligned}
\frac{\partial N_\alpha}{\partial x} - \frac{\partial N_\alpha}{\partial y} &= \frac{4\pi\sqrt{2}\,J_s}{c\Phi_0\varepsilon}\left|\frac{N_\alpha\Phi_0}{cE_0\sqrt{2}}\,(-V_{x\alpha}+V_{y\alpha})\right|^{1/m} \\
&\quad\times \operatorname{sgn}\left[\frac{N_\alpha\Phi_0}{cE_0\sqrt{2}}\,(-V_{x\alpha}+V_{y\alpha})\right], \\
\frac{\partial N_\alpha}{\partial x} + \frac{\partial N_\alpha}{\partial y} &= -\frac{4\pi\sqrt{2}\,J_s}{c\Phi_0\varepsilon}\left|\frac{N_\alpha\Phi_0}{cE_0\sqrt{2}}\,(V_{x\alpha}+V_{y\alpha})\right|^{1/m} \\
&\quad\times \operatorname{sgn}\left[\frac{N_\alpha\Phi_0}{cE_0\sqrt{2}}\,(V_{x\alpha}+V_{y\alpha})\right].
\end{aligned} \tag{37}$$

The critical current J_s depends on the magnetic induction. In the preceding sections, we neglected this dependence, but in this section, we solve the problem near the magnetization-reversal front, where the magnetic induction passes through zero. Near this line, the density of the critical current can change quite sharply. Because the concrete form of the dependence $J_s(B)$ is insignificant for the further analysis, for definiteness, we use one of the dependences frequently encountered at low temperatures, $J_s \propto 1/B$, which can suitably be represented as $J_s = A/N_\alpha$.

We must impose boundary conditions on the sample surface:

$$N_2(d) = N_2(-d) = \frac{|H|}{\Phi_0}\,. \tag{38}$$

The equation for the interface between vortices of different signs can be written as $x = x_0(y,t)$. For the velocity of propagation of this surface $\mathbf{U}(t,y)$, we then obtain

$$U_x = \frac{\partial x_0}{\partial t}\,\frac{1}{1+(\partial x_0/\partial y)^2}\,,\qquad U_y = \frac{\partial x_0}{\partial t}\,\frac{\partial x_0/\partial y}{1+(\partial x_0/\partial y)^2}\,. \tag{39}$$

In the unperturbed state (prior to the appearance of turbulence), the magnetization-reversal front is flat, $x = x_0(t)$, and hence $U_y = 0$.

The condition of the magnetic flux conservation means that the number of annihilating vortices is equal to the number of antivortices, i.e., the fluxes of vortices of the opposite sense are compensated at the interface,

$$N_1(\mathbf{V}_1 - \mathbf{U})_n + N_2(\mathbf{V}_2 - \mathbf{U})_n = 0\,, \tag{40}$$

where the subscript n refers to the components of vectors that are normal to the interface. For the components of the vector normal to this surface, we have

$$v_x = \frac{1}{\sqrt{1+(\partial x_0/\partial y)^2}}\,,\qquad v_y = \frac{\partial x_0/\partial y}{\sqrt{1+(\partial x_0/\partial y)^2}}\,. \tag{41}$$

Following the approach that is commonly accepted in kinetics, we assume that the rate of annihilation of the vortices is proportional to their concentrations and is determined by some phenomenological constant R:

$$N_1(\mathbf{V}_1 - \mathbf{U})_n = R N_1 N_2\,. \tag{42}$$

At the boundary, the magnetic induction passes through zero; we then have

$$N_1 = N_2 = N_0\,. \tag{43}$$

We note that this condition follows automatically from Eqns (33) and (40) and from the initial conditions of the problem. In specifying boundary conditions at the magnetization-reversal front, we used two assumptions, which are confirmed experimentally. The first states that the thickness of the region in which the annihilation of vortices occurs is small compared to the other characteristic scales. The second assumption is that the density of vortices and antivortices in this region changes almost jumpwise (according to the estimates and experimental data, $\Phi_0 N_1 \sim H_{c1}$). These approximations are discussed in [75] in more detail.

The set of equations (33), (37) with boundary conditions (38), (40), (42), and (43) has a stationary solution:

$$N_\alpha(x) = N_0\sqrt{1+s_\alpha C(x_0 - x)/d}\,,\qquad C = \frac{8\pi\sqrt{2}\,dA}{c\Phi_0 N_0^2}\left[\frac{\sqrt{2}\,\Phi_0 R N_0^2}{cE_0(1+\varepsilon^m)}\right]^{1/m} \tag{44}$$

and $U = 0$. In the experiments that are of interest for us, the density of vortices near the zero-induction surface, N_0, is much lower than that at the boundaries of the sample, and therefore the unity in the radicand in (44) can be neglected. Taking into account that $\varepsilon^m \ll 1$, we then obtain the following estimate for the density of vortices at the magnetization-reversal front:

$$N_0 = N_\alpha(x = x_0) \sim \left(\frac{|H|}{H_p}\right)^m \left(\frac{cE_0}{2^{(m+1)/2}\Phi_0 R}\right)^{1/2},\qquad H_p = \left(\frac{8\pi d A \Phi_0}{c}\right)^{1/2}. \tag{45}$$

We are certainly interested in a nonstationary solution of the above equations. But it can be shown that if the velocity of the front is much lower than the velocity of vortices in the sample volume, $U \ll V_\alpha$, then the above stationary equation is a first approximation for a nonstationary solution.

We introduce the dimensionless variables

$$n_\alpha = \frac{N_\alpha}{N_0}\,,\quad \tau = \frac{t}{t_0}\,,\quad t_0 = \frac{\Phi_0^2 N_0^3}{8\pi A E_0}\,,\quad \xi = \frac{x}{L}\,,\quad \zeta = \frac{y}{L}\,,\quad L = \frac{c\Phi_0 N_0^2}{4\pi\sqrt{2}\,A}\,,\quad r = \frac{R N_0^2 \Phi_0}{\sqrt{2}\,cE_0}\,,\quad u = \frac{U t_0}{L}\,. \tag{46}$$

For normalization, we use the density of vortices at the uncurved front, $N_0 = N_\alpha(x_0(t))$. We suppose that this quantity changes on time scales that are much greater than the characteristic time of the instability development. Assuming that the velocity of the magnetization-reversal front is small, we can linearize the equations with respect to this quantity. As a result of simple transformations, we obtain

$$n'_\alpha(x = x_0) = -s_\alpha p\left(1 + s_\alpha\,\frac{u}{rm}\right),\qquad n''_\alpha(x = x_0) = -(n'_\alpha)^2 - \frac{2u}{(1+\epsilon)\,m(n'_\alpha)^{m-2}}\,,\qquad \epsilon = \varepsilon^m\,,\quad \rho = \left(\frac{2r}{1+\epsilon}\right)^{1/m}, \tag{47}$$

where the prime denotes differentiation with respect to the dimensionless coordinate ξ.

To investigate the stability of the solution, we represent the density of vortices in the form of a sum of an unperturbed solution of the problem with a flat interface $\tilde{n}_\alpha(\xi,\tau)$ and a small perturbation,

$$n_\alpha = \tilde{n}_\alpha + f_\alpha\big(\xi - \xi_0(\tau)\big)\exp\left(\lambda\tau + \mathrm{i}k\zeta\right). \tag{48}$$

A boundary conditions must be imposed on the perturbed interface:

$$\xi = \xi_0(\zeta, \tau) = \xi_0(\tau) + \delta\xi \exp(ik\zeta + \lambda\tau) . \quad (49)$$

It follows from condition (40) that $\delta\xi = (f_1 - f_2)/2\rho$. Substituting (48) in continuity equation (33), we obtain linear equations for the perturbations f_α:

$$f_\alpha'' + 2f_\alpha'\left[ik(1-2\epsilon) + \frac{\tilde{n}_\alpha'}{\tilde{n}_\alpha} - u\,\frac{m-2}{m\tilde{n}_\alpha'^{(m-1)}\tilde{n}_\alpha^m}\right] - \frac{2\lambda}{m\tilde{n}_\alpha'^{(m-1)}\tilde{n}_\alpha^m} - \frac{2u}{\tilde{n}_\alpha'^{(m-2)}\tilde{n}_\alpha^{m+1}} - \frac{2uik(m-1)}{m\tilde{n}_\alpha'^{(m-1)}\tilde{n}_\alpha^m} - \frac{\tilde{n}_\alpha'^2}{\tilde{n}_\alpha^2} - k^2 + 2ik\,\frac{\tilde{n}_\alpha'}{\tilde{n}_\alpha} = 0 . \quad (50)$$

Assuming that the perturbations rapidly decay far from the interface between the vortices and antivortices, we replace the functions $\tilde{n}_\alpha(\xi)$ and $\tilde{n}_\alpha'(\xi)$ with their values at the unperturbed boundary $\xi = \xi_0$. As a result, we obtain

$$f_1(\xi - \xi_0) = f_1 \exp\left[p_1(\xi - \xi_0)\right] , \quad f_2(\xi - \xi_0) = f_2 \exp\left[p_2(\xi - \xi_0)\right] , \quad (51)$$

where

$$p_{1,2} = \pm\rho - ik + \frac{\rho u}{2r} \pm \Omega_{1,2} , \quad (52)$$

$$\Omega_{1,2} = \left[2\rho^2 + \frac{iku\rho}{mr} + 4\epsilon k^2 \mp \frac{iku\rho(m-1)u}{m^2r^2} \pm \frac{2u\rho^2}{mr} \mp \frac{\lambda\rho(m-1)u}{m^2r^2}\right]^{1/2}, \qquad \mathrm{Re}\,\Omega_{1,2} > 0 . \quad (53)$$

Now, substituting relations (51)–(53) in boundary conditions (40) and (42), we obtain a set of two linear homogeneous algebraic equations for the amplitudes f_1 and f_2. Equating the determinant of this set of equations to zero, we find the equation for the instability-growth increment $\lambda(k)$. Neglecting the terms of the order of u^2, we write this equation in the form

$$\lambda = \frac{mr}{\rho}\left(\Omega^2 - 4\epsilon k^2 - iku\,\frac{\rho}{mr} - 2\rho^2\right) , \quad (54)$$

where Ω is the root of the equation

$$\Omega^4 + \Omega^3\rho\,\frac{m+2}{m} - 2\Omega^2\rho^2\,\frac{m-1}{m} - 4\Omega\,\frac{\rho^3}{m} - iku\,\frac{\rho}{m^2r}\left(\Omega^2\,\frac{m-1}{2} + \Omega\,\frac{\rho m}{2} + \rho^2 m\right) - 4\epsilon k^2\left(\Omega^2 + \Omega\,\frac{2\rho}{m} + iku\,\frac{\rho(m-1)}{2m^2r}\right) = 0 , \quad (55)$$

with $\mathrm{Re}\,\Omega > 0$.

If $m = 1$, the sample has a purely ohmic conductivity, which is not characteristic of superconductors. But this case is interesting from the methodological standpoint. It has been analyzed in detail in [72]. We give the results of the analysis of Eqns (54) and (55) at $m = 1$. These equations have a solution with $\mathrm{Re}\,\lambda > 0$ if $\varepsilon \ll 1$. In this case, $k \gg 1$. The maximum value of the instability-growth increment λ_m and the corresponding value of k_m are

$$\mathrm{Re}\,\lambda_m \approx \frac{|u|r}{8\varepsilon^{1/2}} - 4r^2 , \qquad k_m \approx \frac{(|u|r)^{1/2}}{(4\varepsilon)^{3/4}} . \quad (56)$$

The existence of solutions with $\mathrm{Re}\,\lambda > 0$ and $k \gg 1$ implies an instability of the flux that is homogeneous along the flow axis, a distortion of the magnetization-reversal front, and the turbulization of the flow [71]. The characteristic spatial scale of the turbulence, l_c, at the initial stage of its development is determined by the most rapidly growing perturbations, $l_c \sim 1/k_m$. The instability arises only if the current anisotropy $1/\varepsilon$ is large:

$$\varepsilon \leqslant 0.019\left(\frac{U}{2RN_0}\right)^2 \ll 1 . \quad (57)$$

This is a very rigid restriction.

We now consider the case $m \gg 1$, which is more suitable for the description of a real experiment (for HTSCs at temperatures at which the instability is observed, m is usually > 10). The parameter $\epsilon = \varepsilon^m$ in Eqn (55) is then negligibly small and the equation takes the form

$$X^4 + \frac{m+2}{m}\,X^3 - 2\,\frac{m-1}{m}\,X^2 - \frac{4}{m}\,X + i\kappa\left(\frac{m-1}{m}\,X^2 + X + 2\right) = 0 , \quad (58)$$

$$X = \frac{\Omega}{\rho} , \qquad \kappa = \frac{k|u|}{2mr\rho} .$$

If $k \gg 1$,

$$X \approx \kappa^{1/2}\exp\left(-\frac{i\pi}{4}\right) - \frac{1}{2m} - \frac{2}{\kappa^{1/2}}\exp\left(-\frac{i\pi}{4}\right) . \quad (59)$$

The instability-growth increment

$$\lambda \approx mr\rho\left(i\kappa + 2 - \frac{\kappa^{1/2}}{2^{1/2}m}\right) \quad (60)$$

has a large imaginary part. This means that the instability grows on the background of oscillations of the electromagnetic field perturbations, which is indeed observed experimentally. The most important fact is that at $m \gg 1$, the instability can arise at a relatively low anisotropy. A numerical analysis of Eqns (54) and (55) shows that for each set of values of the parameter m and of the ratio u/r, a critical value of the anisotropy parameter ε_c exists: if $\varepsilon > \varepsilon_c$, the magnetization-reversal front is stable; if $\varepsilon < \varepsilon_c$, macroturbulence develops.

We note that in single crystals of $1-2-3$ HTSCs, a significant anisotropy of the critical current exists even after the crystals are subjected to the twin elimination procedure [76]. Therefore, it is not surprising that macroturbulence can also arise in such single crystals. However, no turbulence is observed in the presence of crossed twins in the sample or in melt-textured materials, in which the density of microcracks and microinclusions is large [63].

3.4 Self-organized dynamic vortex structures arising on defects

Above, when speaking of HTSCs, we discussed dynamic vortex structures arising in single crystals. But the extended

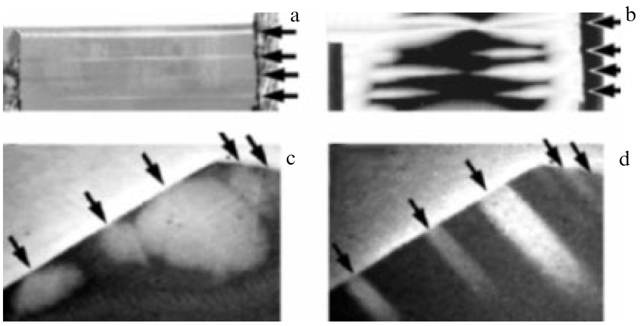

Figure 8. Influence of defects on the magnetic flux penetration into a superconductor. (a) Twinned structure of the YBCO plate and (b) related inhomogeneous penetration of the flux (the twin boundaries are indicated by arrows; it can be seen that the flux penetrates much more deeply along these boundaries). (c, d) Defects at the edge of the crystal (their positions are shown by arrows) and their effect on the penetration of the flux: (c) penetration of a perpendicular magnetic flux into a BSCCO plate at a temperature $T < 30$ K, $H_z = 58$ Oe; and (d) a tilted field $H_{ab} = 432$ Oe, $H_z = 77$ Oe (the penetration of the flux begins from the defects at the edge of the sample; the perpendicular field penetrates in the form of inflating bubbles; the tilted field penetrates in the form of bands).

defects characteristic of these systems can also lead to quite a peculiar picture of the magnetic flux penetration [77–83].

Figures 8a and 8b illustrate the penetration of the magnetic flux into a YBCO sample with a developed system of twins. As can be seen, the magnetic field penetrates into the sample volume to a much greater depth along twin boundaries. Figures 8c and 8d show the penetration of a transverse magnetic flux into a BSCCO (BiSrCaCuO) single crystal [82]. The vortices penetrate into the sample through defects located near the edge of the plate. If the sample is placed in a constant magnetic field oriented in the sample plane (the *ab* plane), then the vortices are aligned along the field direction at low temperatures. At temperatures above 30 K, temperature fluctuations break the Josephson coupling between the CuO planes and the in-plane magnetic field stops affecting the distribution of the magnetic flux component directed along the *c* axis.

Peculiar dynamic effects can also be observed on extended defects. As an example, we discuss structures in the form of 'droplets' (or 'bubbles') and rows of such droplets ('beads'), which have been observed in a magnetooptical study of the dynamics of the magnetic flux in single crystals of $Bi_2Sr_2CaCu_2O_8$ (B2212) (Fig. 9). The droplets and beads

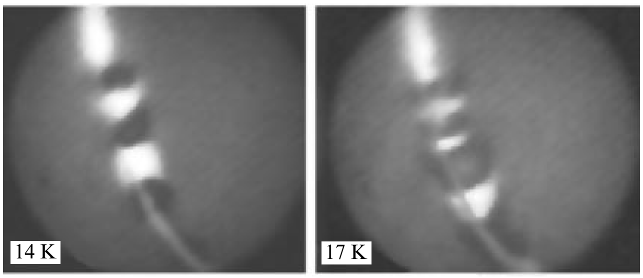

Figure 9. Alternating macroscopic magnetic-flux droplets nucleated in BSCCO on a linear defect upon the cyclic magnetization reversal of the sample by a variable magnetic field perpendicular to its plane at temperatures (a) 14 K and (b) 17 K. The dark and light droplets (beads) correspond to opposite-sense fluxes.

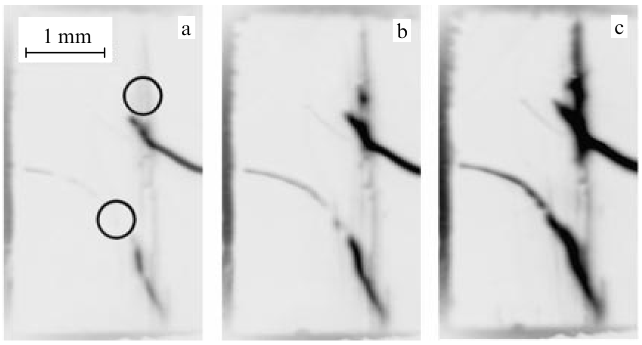

Figure 10. Magnetooptical image of a B2212 single crystal in a constant transverse magnetic field at $T = 15$ K: (a)–(c) correspond to an increasing magnetic field. The dark regions are occupied by the magnetic flux. The circles in (a) show the places where bubbles are pumped up in a variable magnetic field.

arise in certain parts of a sample placed in a low-frequency transverse magnetic field.

High-quality B2212 single-crystal plates have been investigated in experiments. If the crystal is placed in a transverse constant magnetic field H_a, then at low temperatures ($T < 30$ K), the magnetic flux penetrates into the sample equally from all faces. At $T > 30$ K, the interplane correlation in B2212 is lost, the force of pinning decreases sharply, and the flux is distributed uniformly over the single crystal in a few fractions of a second. A more detailed study of the penetration of a magnetic flux into a sample in low fields shows that at the initial stage, the vortices move into the bulk along several characteristic planar defects that are parallel to the crystallographic *c* axis. These defects are invisible optically, but are clearly visible in magnetooptical images. In Fig. 10, the dark regions are occupied by the magnetic flux. There are also some points at which a coarse defect intersects with a finer one, which can be visible only at larger magnification. These points are circled in Fig. 10. Precisely at these points, which we call 'weak' points for brevity, dynamic structures of the magnetic flux in the form of droplets arise.

At $T < 30$ K, if we increase a constant magnetic field such that the front of the magnetic flux penetration along the defect approaches a weak point, we see that the magnetic flux accumulates near this point with time. Figure 11 shows the time dependence of the magnetic induction B at a weak point. It can be seen that B grows (the lower curve), whereas in the

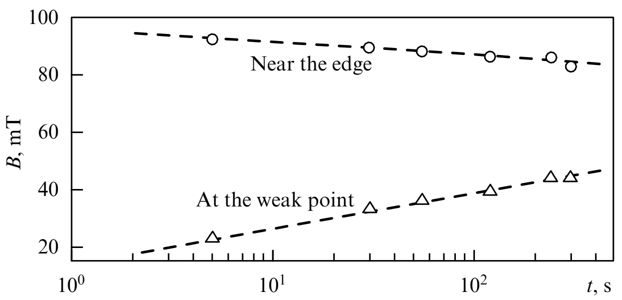

Figure 11. Time variation of the magnetic induction $B(t)$ in a constant magnetic field of 460 Oe applied to a B2212 plate at $T = 13$ K near the edge of the sample (circles) and in the center of a weak point (triangles).

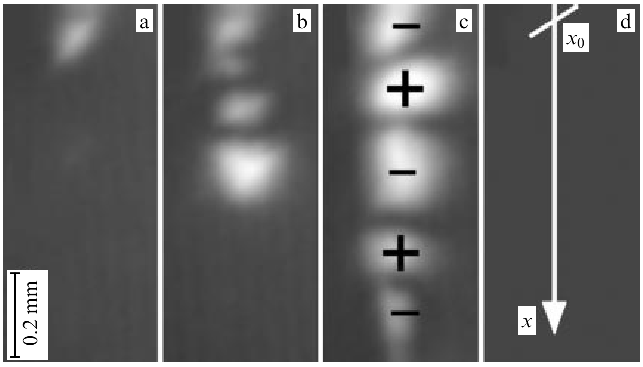

Figure 12. Alternating macroscopic magnetic flux droplets in a BSCCO single crystal, which are nucleated at a linear defect near a weak point when pumped up by a variable magnetic field (amplitude 250 Oe, frequency 15 Hz, temperature 18 K) perpendicular to the sample plane: (a) nucleation of a droplet; (b, c) patterns after many cycles of field variation; and (d) a planar defect with a weak point (schematic) [81].

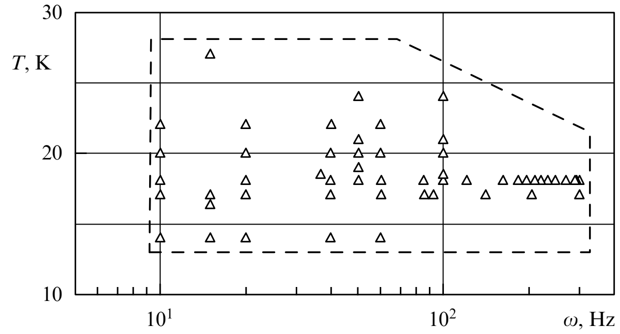

Figure 13. Region on the (T, ω) plane in which the pumping of bubbles is observed.

planar defect near the face, the magnetic field decreases (the upper curve). This means that superconductivity at the weak point is markedly suppressed.

We assume that the external field oscillates with a low frequency ω and small amplitude, $H_a(t) = H_0 \cos(\omega t)$. Let the field amplitude be such that the magnetic flux penetrates into the volume only along the defects and the flux penetration front is located near a weak point (Fig. 12). At very low frequencies, the magnetic flux changes sign along with the external field at all points of the sample. As the field frequency exceeds 10 Hz, the picture changes noticeably. The magnetic flux of a certain sign starts pumping near the weak point (Fig. 12a). The size of the arising macroscopic vortex bubble grows as the number of cycles of the magnetic field increases, and the magnetic induction increases in its center. The bubble 'breathes,' following changes in the magnetic field: the size of the bubble and the magnetic induction in it are greater when the sign of the external field coincides with the sign of the accumulating magnetic flux. When the size of the bubble reaches a certain critical value, the bubble breaks away from the weak point, losing part of the trapped magnetic flux, and shifts along the linear defect more deeply into the sample. At the weak point, a bubble with the flux of the opposite sign starts blowing up; and so on. As a result, a structure of macroscopic vortex droplets of alternating sign is aligned along the defect, resembling beads (Figs 12b, 12c).

This effect of self-organization is reproduced and observed at each weak point localized at a linear defect. The above-described process of the formation of droplets resembles the effect of generation of domain walls and Bloch lines in ferromagnets [84–86] and the effect of pumping a magnetic flux into type-I superconductors [87].

The pumping of bubbles is observed in a limited range of amplitudes and frequencies of the magnetic field and only in some range of temperatures. The region in which this phenomenon exists in the (T, ω) plane is shown in Fig. 13. The region of temperatures in which this effect is observed is $12 < T < 30$ K. At higher temperatures, the magnetic flux penetrates easily into the HTSC bulk rather than moves along the defect. The region of frequencies in which the bubbles arise is from 10 to approximately 100–300 Hz (depending on temperature).

The fact that the droplets are formed in some range of field amplitudes is rather obvious. Indeed, for a droplet to be formed, the field amplitude must be sufficiently high for the magnetic flux to approach close to a weak point. But if the amplitude is too large, a weak point occurs behind the front of the penetrating magnetic flux. In this case, upon the change in the sign of the magnetic flux, vortices of opposite signs freely approach the weak point and annihilate with the vortices already existing there.

A model for the description of the effect of pumping-up of bubbles was suggested in [80, 81]. The vortices moving along a planar defect produce a magnetic field $\mathbf{B}_v$, which depends on the coordinate along the defect and on time. Outside the defect, $\mathbf{B}_v = 0$. We assume that in the vicinity of a weak point located at $x = x_0$, superconductivity is suppressed to zero in the region $x_0 < x < x_0 + \Delta x$. The planar defect intersects the sample face at $x = 0$. The position of the magnetic flux front at a given field amplitude is denoted by $x_1(H_a)$. Let $x_1 - x_0 \ll x_0$.

After the first half-cycle of the field variation, some number of vortices fall into the weak point due to the thermoactivational creep of the magnetic flux (TCMF) and become trapped there. The TCMF rate is proportional to $\exp(-U/k_B T)$, where U is the height of the corresponding potential barrier and k_B is the Boltzmann constant. To move out from the weak point, the vortices must overcome a higher barrier $U + \Delta U$, because the residence of vortices at the weak point is energetically more favorable. The vortices can accumulate at a weak point only if the ratio $U/k_B T$ is not too large. If the temperature is too low, the TCMF rate is small and no accumulation of vortices is observed, at least in a reasonable experimental time. On the contrary, for vortices that accumulate at a weak point, it is necessary that $U + \Delta U \gg k_B T$. It is clear from this consideration why the pumping of magnetic flux bubbles occurs only in a certain temperature window.

Upon the change in the sign of the field, the front of the penetration of opposite-sign vortices (antivortices) also occurs at the position x_1. The antivortices come into the droplet due to the TCMF; the annihilation of opposite-sign vortices prevents the growth of the droplet. Consequently, we have to conclude that the pumping-up of a droplet is possible only if the potential barrier U_f for the introduction of vortices into a weak point (i.e., for a flux with the same polarization as in the case of the previously trapped flux) is smaller than the barrier U_a for the antivortices (i.e., for the opposite-polarization flux).

The barrier U consists of three terms: a contribution from the pinning forces (U_p), a contribution from shielding currents (U_v), and a contribution from the stray magnetic field (U_{m}), which arises due to the nonzero demagnetizing factor of the sample. The contribution from the pinning is independent of the mutual polarization of the vortices and cannot therefore be responsible for the effect of the pumping up of the droplets. This term grows rapidly with increasing the distance between the weak point and the front of the flux. Therefore, the observation of the pumping-up of the droplets is possible only if the distance $x_0 - x_1$ is sufficiently small. The contribution to the barrier U_{v}, which arises due to the interaction of vortices with shielding currents, also includes, in particular, the interaction between the vortices. Vortices of the same polarization repel one another; vortices with opposite polarizations are attracted to one another. Consequently, this term stimulates the entering of antivortices into the droplet and their annihilation. However, the interaction between the vortices decays exponentially at distances of the order of the London penetration depth λ. For the B2212 HTSC in the *ab* plane, this distance is about 200 nm. In experiments, the characteristic scale $x_0 - x_1$ exceeds λ_{ab} by about three orders of magnitude (see Fig. 12). It is obvious that the role of the quantity U_{v} is insignificant under the experimental conditions.

The contribution to the barrier from stray fields, U_{m}, depends on the mutual orientation of the vortices in the droplet and in the front of the entering flux (Fig. 14). By analogy with domains in ferromagnets, the magnitude of stray fields is smaller if the magnetic fluxes in the droplet and at the front have opposite signs. Superconductors are diamagnetic and their magnetic moments decrease when a magnetic flux enters the sample. Consequently, U_{m} is negative, which leads to a decrease in the barrier. The entering of fluxes into the droplet leads to a decrease in the total magnetic moment of the sample; the entering of antivortices and annihilation lead to a decrease in the magnetic induction in the droplet and hence to an increase in the energy of the stray magnetic fields. Therefore, precisely the energy of stray fields, or the magnetostatic energy, is responsible for the pumping of droplets.

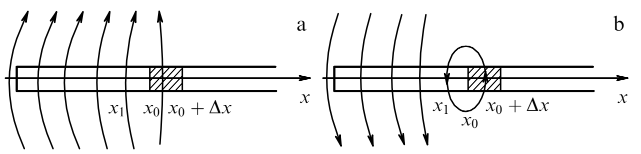

Figure 14. Stray magnetic fields near a weak point ($x = x_0$) and near the front of the magnetic flux ($x = x_1$): (a) the directions of the magnetic induction in the droplet and at the front are coincident; and (b) the induction directions in the droplet and at the front are opposite.

To illustrate, we consider the following simplified model. Let the distributions of the magnetic field for the configurations shown in Figs 14a, 14b be coincident except in some region near the weak point. We let $\mathbf{H}_0(x)$ denote coincident contributions to the magnetic field. The magnetic flux trapped at the weak point produces field $\pm\mathbf{H}_{\mathrm{in}}(x)$, where the plus sign corresponds to a flux–flux configuration and the minus sign corresponds to a flux–antiflux configuration. The Gibbs energy for these two configurations can be written as

$$\mathcal{F} = \int_V \mathrm{d}V \left\{ \frac{\left[\mathbf{H}_0(x) \pm \mathbf{H}_{\mathrm{in}}(x)\right]^2}{8\pi} - \frac{\left[\mathbf{H}_0(x) \pm \mathbf{H}_{\mathrm{in}}(x)\right]\mathbf{H}_{\mathrm{a}}}{4\pi} \right\}, \tag{61}$$

where the upper signs (pluses) correspond to the flux–flux case and the lower signs (minuses), to the flux–antiflux case, $\mathbf{H}_{\mathrm{a}}$ is the external field, $\mathbf{H}_{\mathrm{a}} = \mathbf{H}_0(x)$ as $x \to \infty$, and the integration is performed over the entire space.

Let a small number of vortices (a small magnetic flux $\delta\Phi$) move from a point x, which is close to x_1, to the weak point. In this case, the field changes by $\delta\mathbf{H}_{\mathrm{ff}}$ or $\delta\mathbf{H}_{\mathrm{af}}$ in the respective flux–flux or flux–antiflux cases. The new distributions of the magnetic fields are $\mathbf{H}_0 + \mathbf{H}_{\mathrm{in}} + \delta\mathbf{H}_{\mathrm{ff}}$ or $\mathbf{H}_0 - \mathbf{H}_{\mathrm{in}} + \delta\mathbf{H}_{\mathrm{af}}$. Then the quantities U_{m} in the two cases under consideration are written as

$$\begin{aligned} U_{\mathrm{ff}}^{\mathrm{m}} &= \mathcal{F}_{\mathrm{ff}}(\mathbf{H}_0, \mathbf{H}_{\mathrm{in}}, \delta\mathbf{H}_{\mathrm{ff}}) - \mathcal{F}_{\mathrm{ff}}(\mathbf{H}_0, \mathbf{H}_{\mathrm{in}}, 0)\,, \\ U_{\mathrm{af}}^{\mathrm{m}} &= \mathcal{F}_{\mathrm{af}}(\mathbf{H}_0, \mathbf{H}_{\mathrm{in}}, \delta\mathbf{H}_{\mathrm{af}}) - \mathcal{F}_{\mathrm{af}}(\mathbf{H}_0, \mathbf{H}_{\mathrm{in}}, 0)\,. \end{aligned} \tag{62}$$

We subtract the second equation from the first and neglect terms that are quadratically small in $\delta\Phi$. Using (61), we then obtain

$$\begin{aligned} U_{\mathrm{ff}}^{\mathrm{m}} - U_{\mathrm{af}}^{\mathrm{m}} = \int_V \frac{\mathrm{d}V}{4\pi} \big[&\mathbf{H}_{\mathrm{in}}(\delta\mathbf{H}_{\mathrm{ff}} + \delta\mathbf{H}_{\mathrm{af}}) \\ &- (\mathbf{H}_{\mathrm{a}} - \mathbf{H}_0)(\delta\mathbf{H}_{\mathrm{ff}} - \delta\mathbf{H}_{\mathrm{af}}) \big]\,. \end{aligned} \tag{63}$$

As is easy to see from the comparison of Figs 14a and 14b, the inequality

$$\left| \int_V \frac{\mathrm{d}V}{4\pi}\, \delta\mathbf{H}_{\mathrm{ff}} \right| \gg \left| \int_V \frac{\mathrm{d}V}{4\pi}\, \delta\mathbf{H}_{\mathrm{af}} \right| \tag{64}$$

holds. The integral

$$\left| \int_V \frac{\mathrm{d}V}{4\pi}\, (\mathbf{H}_{\mathrm{a}} - \mathbf{H}_0) \right| \tag{65}$$

has the order of the total diamagnetic moment of the sample, which is much greater than the small contribution produced by the term H_{in}. Therefore, $U_{\mathrm{ff}}^{\mathrm{m}} - U_{\mathrm{af}}^{\mathrm{m}} < 0$, which means a pumping-up of bubbles.

3.5 Twisters

The process of magnetization of type-I superconductors in crossed fields is quite peculiar because of the appearance of vortices with different orientations of the magnetic flux. We here note a nontrivial effect such as the collapse of magnetization, or the suppression of the constant magnetic moment of the superconductor under the effect of a transverse low-frequency magnetic field [88–91].

In crossed fields, in the $YBa_2Cu_3O_x$ HTSC, peculiar dynamic structures are observed that are called 'twisters' [92, 93]. This effect has been investigated in much detail experimentally [94–96].

Twisters are usually observed in single-crystal samples with a plate-like shape. At a temperature above T_{c}, the sample is placed in a constant magnetic field H_{dc} in the plate plane (the crystallographic *ab* plane). Then the sample is cooled to a specified temperature $T < T_{\mathrm{c}}$ and is placed in a transverse magnetic field $H_{\mathrm{tr}} < H_{\mathrm{dc}}$. The transverse magnetic flux enters the plate anisotropically: it enters to greater distances along the in-plane field and to smaller distances across the in-plane field (Figs 15a, 15b). The extent of the anisotropy depends on the value of the in-plane field and on temperature. The greater H_{dc} is, the stronger the asymmetry. When the transverse field varies between $+H_{\mathrm{tr}}$ and $-H_{\mathrm{tr}}$, a picture arises resembling the formation of bubbles on defects described in Section 3.4.

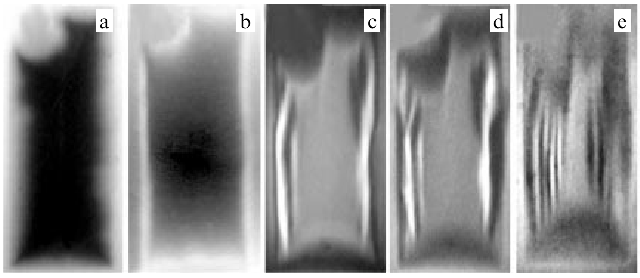

Figure 15. Magneto-optical images of the magnetic induction distribution in a YBCO single crystal at $T = 36$ K: (a) constant transverse magnetic field $H_{tr} = 1280$ Oe; (b) asymmetric pattern of the penetration of a tilted field; the constant field in the sample plane $H_{dc} = 1250$ Oe; the transverse field $H_{tr} = 250$ Oe; along the field lines of the in-line field H_{dc} (applied vertically in the figure), the flux penetrates much more deeply than across the lines; (c, d) flux penetration patterns after several cycles of the variation of the transverse field ($-250 < H_{tr} < 250$ Oe); (e) after cycling in H_{tr} with a frequency of 100 Hz for 10 s. Dark and bright bands along the longer sides of the sample show the distribution of the alternating transverse magnetic flux trapped in the plate.

Near the edges of the plate (parallel to the in-plane field), a gradual accumulation of the transverse magnetic flux occurs cycle after cycle. After the band with the trapped flux reaches some critical width, it breaks away from the plate edge and the pumping of a band with a transverse flux of another sign starts, and so on. (Figs 15c, 15d). With time, the bands become numerous. They move to the plate center, where they annihilate (Fig. 15d). Twisters are formed when the transverse field amplitude exceeds some threshold value. With increasing the field amplitude, the process of the penetration of twisters into the crystal first becomes periodic, but then, at greater amplitudes, becomes stochastic. Twisters are observed in the temperature range from 20 to 70–75 K in single crystals of $YBa_2Cu_3O_x$ with a high and low density of twins [94–96]. In HTSCs with a higher crystallographic anisotropy (e.g., in BSCCO or $YBa_2Cu_4O_x$), no twisters have been revealed.

The nature of twisters has not been understood completely. Supposedly, they are formed by helical Abrikosov vortices (hence the name 'twister') that arise because of the intersection of vortices lying in the *ab* plane and vortices directed transversely to the plate, along the *c* axis [92]. This follows from the fact that twisters are absent in BSCCO, where Josephson vortices lie in the plane and stacks of two-dimensional vortices (pancakes) are formed in the transverse direction. It is clear that the mechanism of the self-completion of this dynamic structure (i.e., the formation of bands with alternating polarization and their dynamics) should also include the effects related to stray magnetic fields, as in the case of bubbles or droplets (see the preceding section). The construction of a theoretical model of twisters requires further investigations.

4. Dynamic effects in ferromagnets

Ferromagnets have spontaneous magnetization; magnetic domains in them arise without the application of an external magnetic field. The domain structure in ferromagnets can be equilibrium or metastable. The form of the equilibrium domain structure can be found by minimizing the free energy (although such a calculation is quite complicated in many cases). It is well known that the period of the domain structure is determined by the balance of several components: the exchange energy W_e, the magnetostatic energy W_m, the energy of crystallographic anisotropy W_a, and the Zeeman energy W_H [97, 98]. The energy of exchange interaction determines the mutual orientation of spins of closely spaced atoms and leads to the appearance of a spontaneous magnetization M_s in macroscopic regions of the ferromagnet. The energy of the crystallographic anisotropy determines the direction of the spontaneous magnetization vector $\mathbf{M}_s$. The magnetostatic energy is the energy of stray fields. Precisely the minimization of this energy determines the partitioning of the magnet into domains. And, finally, in an external magnetic field, a Zeeman term appears, which describes the interaction of magnetic moments with the external magnetic field.

Just as in superconductors, in the dynamics of rapid magnetization reversal, states can form in ferromagnets that dramatically differ from those that arise under quasistatic conditions [99–105]. The appearance of such magnetic structures changes the macroscopic characteristics of the material, leading to magnetization jumps, increasing noise, etc. The dynamic structures in ferromagnets are quite various. Here, we describe only those that are analogous to some dynamic magnetic structures in superconductors.

The examples of the transformation of a static domain structure under the effect of a variable magnetic field are shown in Fig. 16. As is known [98], a labyrinthine domain structure (Fig. 16a), whose period is determined by the material parameters and the thickness of the film, is formed in films with a perpendicular anisotropy. In a variable field, such a structure begins 'breathing' (its boundaries oscillate synchronously with the field), and the structure can change its type under certain conditions [99] (Fig. 16b). In the presence of macroscopic point defects, spiral-like structures can appear in ferromagnetic films that are not observed in the case of quasistatic magnetization reversal [100, 101] (Figs 16c, 16d). Such types of dynamic structures arise in a limited range of amplitudes and frequencies of the exciting field, just like magnetic flux droplets in HTSCs (see Section 3.4). A detailed description of the variety of spiral structures in ferromagnetic films can be found in [100].

A closer analogy to the nucleation of macroscopic droplets of magnetic flux in HTSCs is provided by the effect of nonresonance generation of Bloch lines in films and thin plates of iron garnets [106–110]. Figure 17a shows a Bloch domain wall separating domains with antiparallel magnetization vectors in the plate plane, which are parallel to the domain wall. Three segments of the wall can be seen (the directions of the magnetization in the center of the wall are

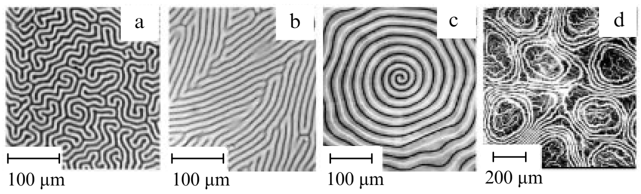

Figure 16. Transformation of the static domain structure under the effect of a variable field in ferromagnetic films: (a) labyrinthine magnetic structure without a field; (b) reorientation of the structure after the application of a variable magnetic field; (c, d) spiral magnetic domain structures arising upon the excitation of the films by a variable magnetic field (borrowed from [100]).

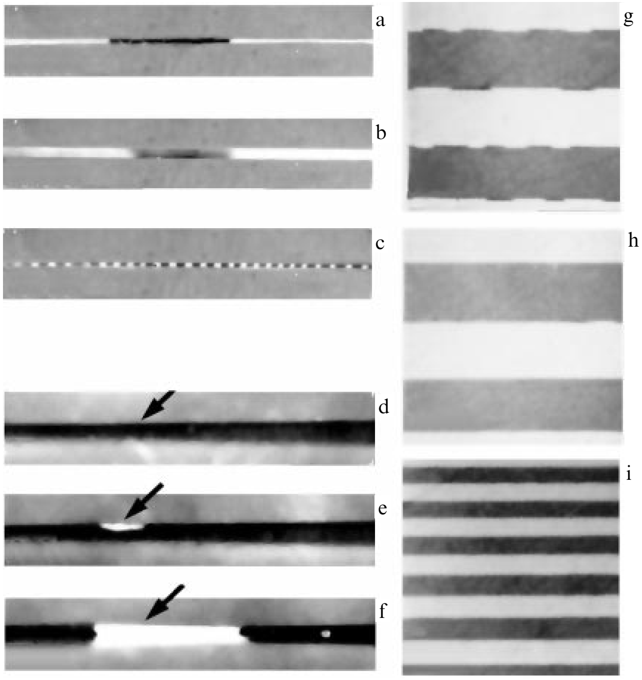

Figure 17. Variation of the structure of a domain wall under the effect of a variable magnetic field directed along the easy axis lying in the plate plane: (a) the wall prior to the switching-on of the field; (b) the wall moving with the speed $\sim 6\ \mathrm{m\ s^{-1}}$; (c) structure of the wall after a long-term excitation by a variable field (density of Bloch lines increased severalfold); (d) an enhanced dark segment of the wall (the arrow shows the position of the point defect at the wall); (e) nucleation of a new segment of the wall at a defect (white on black); (f) an overgrown segment of the wall (white). Variation of the domain structure under the effect of a variable magnetic field: (g) static structure; (h) after the switching-on of a variable field perpendicular to the domain walls and to the easy axis; (i) the same region of the structure after switching-off of the exciting field. The scale in (a)–(c) is 100 μm; in (d)–(f), 20 μm; in (g)–(i), 200 μm. Photos (d)–(f) are courtesy of V S Gornakov.

opposite in the white and black segments). The application of a variable magnetic field leads to the excitation in the domain wall of small-amplitude oscillations of the Bloch lines, synchronous with the field (shifts of the walls between the segments, Fig. 17b); near point defects, local oscillations of the magnetization vector are observed, also synchronous with the field.

After many cycles of the variation of the external field, a kink arises at the defect localized on the wall (Figs 17d, 17e): the magnetization vector in the domain wall changes sign. A new segment of the domain wall is formed (Fig. 17f), which grows with time and reaches some critical size, after which a new segment of the domain wall is formed on the defect, now with the other sign. The existing segments of the walls shift and become denser, with some of them annihilating or leaving the wall at the plate edge. As a result, a dense chain of segments with alternating directions of the magnetization vector is formed on the domain wall (Fig. 17c).

This effect is observed in a wide range of frequencies of the exciting field if its amplitude is greater than some critical value h_c. The effect exists at any orientation of the applied magnetic field relative to the plane of the sample. The orientation affects only the value of h_c. The described process of the generation of kinks leads to jumps of the magnetic susceptibility and to increasing dissipation [106, 111].

In ferromagnets, a phenomenon similar to twister HTSCs is also observed. Figure 17g shows a typical regular domain structure in a plate of iron garnet with an in-plane anisotropy. With the application of a variable in-plane magnetic field to the plate, the domain walls and the fine structure of the walls (Bloch lines) start moving (Fig. 17h). However, in a certain range of the magnetic field amplitudes and frequencies [85, 109, 110, 112], a process of generation of new walls at the edge of the plate starts (and at larger amplitudes, also in one or several weak points of the sample); the formation of new walls occurs in a time corresponding to many periods of the oscillations of the exciting field, just as the above-described generation of new Bloch lines in domain walls or as the formation of twisters. The generation of walls is excited if the amplitude of the variable field exceeds some threshold. The threshold value depends on the frequency of the field and on its direction; the rate and the regularity of the generation depend on both the amplitude and the frequency of the field. The dynamics of the process also resemble the dynamics of the generation of twisters. The arising new walls push the already existing walls into the bulk of the plate, and the number of domains therefore increases (Fig. 17i).

If the amplitude of the variable field is of the order of the threshold one, the generation of new walls occurs only rarely and irregularly, and part of the newly formed walls collapse. With increasing the amplitude, the generation becomes more frequent and quasiperiodic, and the newly generated domain walls are irreversibly shifted from the point of generation. A directional drift of domain walls occurs [109]. With increasing the field amplitude, new centers of generation of domain walls arise, and the propagation of walls becomes irregular, random. And, finally, at even greater amplitudes of the variable field, the generation first occurs by discrete trains and then disappears completely. The same picture is observed upon the generation of twisters in HTSCs.

An analogous effect was also observed in films with perpendicular anisotropy upon the pumping by a field with a frequency close to the ferrimagnetic resonance [103]. It has been shown numerically [113] that the formation of new domains can be due to local flip-over of magnetic moments when driven by a resonance field. An analogous process possibly occurs upon the generation of new domain walls, although the frequencies of the driving field are far from the resonance frequencies required for wall motion.

Real crystals always contain defects, which result in inhomogeneities in the concentration of the local magnetostatic field. On such defects, the process of the flip-over of the magnetic moment and generation of pairs of walls (or Bloch lines) can start, and magnetostatic fields then favor their growth and stimulate the motion of the other walls to favor the equalization of the domain structure period. As was already noted, the origin of twisters has not yet been clarified. The discernible analogy between these effects will possibly facilitate the solution of this problem.

With a slow magnetization reversal of plates with a perpendicular anisotropy, the domain walls grow, remaining straight, but then, as the crystal becomes filled by them, they undergo a bending instability (Figs 18a–18c); as a result, a typical labyrinthine domain structure is formed (Fig. 18d). However, in the case of a rapid switching of the magnetic field, the wall growth scenario changes: the new magnetic phase begins growing in the form of branching strips — dendrites (Fig. 19). As was shown in [114], the dendrite-like growing-in of domains is observed in films under a suffi-

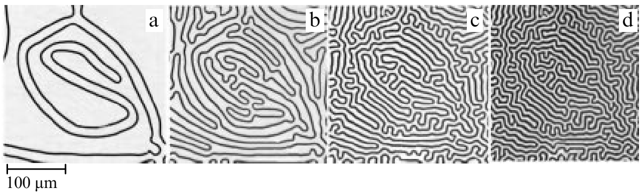

Figure 18. Evolution of magnetic domains in a film with perpendicular anisotropy in the case of a slow decrease in the field from the exciting field (91 Oe) to a minimum value $H_{\min}$: (a)–(d) $H_{\min} = 47.6, 35.7, 18.5$, and 1 Oe, respectively.

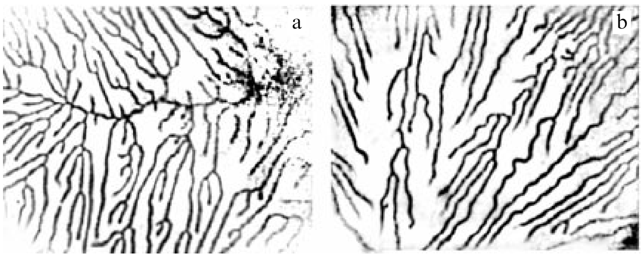

Figure 19. Domain structure of an iron garnet film with a moderate anisotropy upon the evolution of the domain structure from the saturated state: (a) saturation field $H_0 = 102$ Oe; the image was taken in the field $H = 23$ Oe, the sweep frequency of the field $f = 25$ kHz; (b) after saturation to $H_0 = 61$ Oe; the image was taken in the field $H = 24$ Oe, the sweep frequency of the field $f = 6.8$ kHz [114].

ciently rapid field variation, when the domain walls grow-in from an overheated state, i.e., with a significant time delay of the flip-over of the magnetization with respect to the change in the sign of the applied magnetic field. In this case, the hysteresis loops are broadened compared with the quasistatic loops, and the growing-in manifests itself as a giant jump in the magnetization. The velocity of the growing-in walls is close to maximum for a given material. This also suggests a direct analogy with the dendritic instability in superconductors: the dendrites in superconductors cut their way only into the superheated Meissner state and only in the case of a rapid change in the external conditions (generating a sufficiently high electric field). The velocity of growing-in of dendrites in superconductors is also close to the theoretical maximum.

The theory of dendritic instability in superconductors is well developed (see Section 3.2). It is known that this instability has a thermal origin. The rapid growing-in of magnetic domains appears to be also accompanied by significant local heating, because the rapid magnetization reversal necessarily causes dissipation. It is possible that the analogy between the dendritic instability in superconductors and in ferromagnets will allow understanding the mechanism of the formation of dendritic structures in the latter.

As was already noted, in films with a perpendicular anisotropy, the domains form a labyrinthine structure. This structure arises as a result of the bending instability of domain walls caused by the interaction of stray fields [98]. The instability can be temporarily suppressed by either cooling the sample in an in-plane field [86] or keeping one domain wall straight in a gradient magnetic field [115]. In the first case, the curving of the wall occurs upon partial magnetization reversal; in the second case (Fig. 20), it occurs when the gradient of the field becomes lower than the critical one [115, 116].

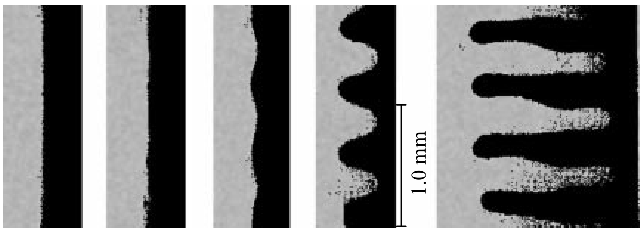

Figure 20. Domain wall straightened by a gradient field in a $Yb_3Fe_5O_{12}$ film with perpendicular anisotropy and the development of a bending instability as a result of a decrease in the gradient [115].

In our opinion, the bending instability has a certain analogy to the development of macroturbulence in HTSCs [61]. To describe the nucleation of a macroturbulence instability in HTSCs, it suffices to use the hydrodynamic approach [72]. However, the further development of macroturbulence should mainly be controlled by magnetostatic interactions at the magnetization reversal front, as in ferromagnets. This analogy can also be useful for understanding the dynamics of the developed phase of macroturbulence.

5. Conclusions

We have seen that instabilities of various natures can arise in type-II superconductors in the mixed state. These instabilities are consequences of the nonlinear electrodynamics of superconductors and of the temperature dependence of the superconductor properties. The instabilities of the superconductor state vary significantly. They lead to the formation of complex spatial magnetic structures, both stationary and dynamic. The study of such processes not only is of great interest from the standpoint of the physics of superconductivity, but also is of great applied importance. For example, just the thermomagnetic instability restricts the current-carrying capacity of commercial superconductors.

The various instabilities of the mixed state have been studied in numerous experimental and theoretical works. As a result, the physical nature of many instabilities has been studied sufficiently well. This concerns, in particular, the thermomagnetic instability (magnetic flux jumps) and the related dendritic instability. The origin of macroturbulence has been clarified; it has been shown that a significant role in the formation of spatial magnetic structures in the mixed state (macroscopic vortex droplets on defects in HTSCs) is played by stray magnetic fields and the thermoactivational creep of the magnetic flux. At the same time, a number of dynamic effects have not yet been given an appropriate physical explanation. First and foremost, this concerns so-called twisters (spatial magnetic structures observed in crossed magnetic fields).

The formation of a spatially inhomogeneous magnetic structure is characteristic of magnetically active media. The best-known examples are domains in ferromagnets. Just as in superconductors, in the process of rapid magnetization reversal in ferromagnets, states that differ from those observed in statics arise. Just as in superconductors, an important role in the dynamics of magnetic structures belongs to dissipation. Dissipation determines the characteristic time of magnetization relaxation (velocity of motion of vortices in superconductors, domain walls in magnets); it determines the heating of the sample in nonstationary processes. Both these factors can substantially affect the characteristic time of the instability development and the spatial structure of the arising inhomogeneous states.

In this review, we emphasized the existing similarities between the dynamic processes that occur under magnetization reversal in ferromagnets and superconductors. An analogy exists between the effects in ferromagnets such as the formation of a labyrinthine magnetic structure and the nonresonance generation of Bloch lines in films and thin plates, on the one hand, and the generation of vortex droplets on defects in HTSCs, on the other hand.

One more example of such an analogy are phenomena that occur in crossed magnetic fields — twisters in HTSC plates and the generation of domain walls in iron–garnet plates with an in-plane anisotropy. It is possible that a physical analogy exists between the nature of the dendritic instability in HTSCs and the effect of the branching growing-in of domain walls in ferromagnets under rapid magnetization reversal, which, in contrast to the dendritic instability, has not yet obtained an appropriate theoretical description. An analogy is also possible between the well-studied bending instability of domain walls in ferromagnetic films with a transverse anisotropy and the development of macroturbulence in HTSCs after the pumping of vortices at the magnetization-reversal front, which leads to the subsequent relaxation of the unstable state via the breakthrough of vortices through the front at the bends. These analogies can be useful for a deeper understanding of the above-described important (and by no means simple) phenomena that govern the macroscopic characteristics of magnetoactive media.

References

1. Bitter F *Phys. Rev.* **38** 1903 (1931)
2. Essmann U, Träuble H *Phys. Lett. A* **24** 526 (1967)
3. Sarma N V, Moon J R *Philos. Mag.* **16** 443 (1967)
4. Vinnikov L Ya et al. *Pis'ma Zh. Eksp. Teor. Fiz.* **90** 325 (2009) [*JETP Lett.* **90** 299 (2009)]
5. Kaczér J *Czech. J. Phys.* **5** 239 (1955)
6. Binnig G, Quate C F, Gerber Ch *Phys. Rev. Lett.* **56** 930 (1986)
7. Martin Y, Wickramasinghe H K *Appl. Phys. Lett.* **50** 1455 (1987)
8. Sáenz J J et al. *J. Appl. Phys.* **62** 4293 (1987)
9. Grütter P et al. *J. Vac. Sci. Technol. A* **6** 279 (1988)
10. Nurgazizov N I, Zhdan P A, Ovchinnikov D V *Pis'ma Zh. Tekh. Fiz.* **34** (11) 74 (2008) [*Tech. Phys. Lett.* **34** 489 (2008)]
11. Giessibl F J *Rev. Mod. Phys.* **75** 949 (2003)
12. Oral A, Bending S J, Henini M *J. Vac. Sci. Technol. B* **14** 1202 (1996)
13. Thiaville A et al. *J. Appl. Phys.* **82** 3182 (1997)
14. Zeldov E et al. *Phys. Rev. Lett.* **73** 1428 (1994)
15. Alers P B *Phys. Rev.* **105** 104 (1957)
16. DeSorbo W *Phys. Rev. Lett.* **4** 406 (1960)
17. Chervonenkis A Ya, Kubrakov N F *Pis'ma Zh. Tech. Fiz.* **8** 696 (1982) [*Sov. Tech. Phys. Lett.* **8** 303 (1982)]
18. Polyanskii A A et al. *Pis'ma Zh. Tekh. Fiz.* **15** (20) 11 (1989) [*Sov. Tech. Phys. Lett.* **15** 872 (1989)]
19. Vlasko-Vlasov V K et al. *Fiz. Nizk. Temp.* **17** 1410 (1991) [*Sov. J. Low Temp. Phys.* **17** 762 (1991)]
20. Indenbom M V et al. *Trans. Magn. Soc. Jpn.* **2** 244 (2002)
21. Jooss Ch et al. *Rep. Prog. Phys.* **65** 651 (2002)
22. Cotton A, Mouton H *Ann. Chim. Phys. 8* **11** 145 (1907)
23. Voigt W *Gött. Nachr. Math.-Phys. Kl.* 355 (1898)
24. Pisarev P V, Sinii I G, Smolenskii G A *Pis'ma Zh. Eksp. Teor. Fiz.* **9** 294 (1969) [*JETP Lett.* **9** 172 (1969)]
25. Faraday M *Philos. Trans. R. Soc. London* **136** 1 (1846)
26. Fowler C A (Jr.), Fryer E M *Phys. Rev.* **104** 552 (1956)
27. Dillon J F *J. Appl. Phys.* **29** 1286 (1958)
28. Ghosh A, Hill W, Fischer P *Phys. Rev. A* **76** 055402 (2007)
29. Nikitin P I, Savchuk A I *Usp. Fiz. Nauk* **160** (11) 167 (1990) [*Sov. Phys. Usp.* **33** 974 (1990)]
30. Kerr J *Philos. Mag. 5* **3** 321 (1877)
31. Williams H J, Foster F G, Wood E A *Phys. Rev.* **82** 119 (1951)
32. Fowler C A (Jr.), Fryer E M *Phys. Rev.* **86** 426 (1952)
33. Hirsch P B et al. *Electron Microscopy of Thin Crystals* (London: Butterworths, 1965) [Translated into Russian (Moscow: Mir, 1968)]
34. Schlenker M et al. *J. Magn. Magn. Mater.* **15–18** 1507 (1980)
35. Schillinger B, Lehmann E, Vontobel P *Physica B* **276** 59 (2000)
36. Pfeiffer F et al. *Phys. Rev. Lett.* **96** 215505 (2006)
37. Kardjilov N et al. *Nature Phys.* **4** 399 (2008)
38. Ovchinnikov S G *Usp. Fiz. Nauk* **169** 869 (1999) [*Phys. Usp.* **42** 779 (1999)]
39. Rogalev A et al. *Lect. Notes Phys.* **697** 71 (2006)
40. Polcarova M, Lang A R *Appl. Phys. Lett.* **1** 13 (1962)
41. Baruchel J, Schlenker M, in *X-Ray and Neutron Dynamical Diffraction: Theory and Applications* (Eds A Authier, Lagomarsino S, B K Tanner) (New York: Plenum Press, 1996) p. 187
42. Mints R G, Rakhmanov A L *Usp. Fiz. Nauk* **121** 499 (1977) [*Sov. Phys. Usp.* **20** 249 (1977)]
43. Mints R G, Rakhmanov A L *Rev. Mod. Phys.* **53** 551 (1981)
44. Gurevich A V, Mints R G, Rakhmanov A L *Fizika Kompozitnykh Sverkhprovodnikov* (The Physics of Composite Superconductors) (Moscow: Nauka, 1987) [Translated into English (New York: Begell House, 1997)]
45. Wertheimer M R, Gilchrist J le G *J. Phys. Chem. Solids* **28** 2509 (1967)
46. Leiderer P et al. *Phys. Rev. Lett.* **71** 2646 (1993)
47. Durán C A et al. *Phys. Rev. B* **52** 75 (1995)
48. Vlasko-Vlasov V et al. *Physica C* **341–348** 1281 (2000)
49. Johansen T H et al. *Europhys. Lett.* **59** 599 (2002)
50. Bobyl A V et al. *Appl. Phys. Lett.* **80** 4588 (2002)
51. Barkov F L et al. *Phys. Rev. B* **67** 064513 (2003)
52. Rudnev I A et al. *Cryogenics* **43** 663 (2003)
53. Yurchenko V V et al. *Phys. Rev. B* **76** 092504 (2007)
54. Albrecht J et al. *Phys. Rev. Lett.* **98** 117001 (2007)
55. Denisov D V et al. *Phys. Rev. Lett.* **97** 077002 (2006)
56. Denisov D V et al. *Phys. Rev. B* **73** 014512 (2006)
57. Rakhmanov A L et al. *Phys. Rev. B* **70** 224502 (2004)
58. Zeldov E et al. *Phys. Rev. B* **49** 9802 (1994)
59. Brandt E H, Indenbom M *Phys. Rev. B* **48** 12893 (1993)
60. Norris W T *J. Phys. D* **3** 489 (1970)
61. Vlasko-Vlasov V K et al. *Physica C* **222** 361 (1994)
62. Vlasko-Vlasov V K et al. *Phys. Rev. B* **58** 3446 (1998)
63. Uspenskaya L S, Naumenko I G, Zhokhov A A *Physica C* **402** 188 (2004)
64. Bass F et al. *Phys. Rev. B* **58** 2878 (1998)
65. Rakhmanov A L et al. *Zh. Eksp. Teor. Fiz.* **122** 886 (2002) [*JETP* **95** 768 (2002)]
66. Vlasko-Vlasov V K et al. *Phys. Rev. B* **56** 5622 (1997)
67. Vlasko-Vlasov V K et al. *Phys. Rev. Lett.* **72** 3246 (1994)
68. Voloshin I F et al. *Zh. Eksp. Teor. Fiz.* **111** 2158 (1997) [*JETP* **84** 1177 (1997)]
69. Frello T et al. *Phys. Rev. B* **59** R6639 (1999)
70. Pastoriza H, Candia S, Nieva G *Phys. Rev. Lett.* **83** 1026 (1999)
71. Landau L D, Lifshitz E M *Gidrodinamika* (Fluid Mechanics) (Moscow: Fizmatlit, 2001) [Translated into English (Oxford: Pergamon Press, 1987)]
72. Fisher L M et al. *Phys. Rev. Lett.* **87** 247005 (2001)
73. Fisher L M et al. *Phys. Rev. Lett.* **92** 037002 (2004)
74. Brandt E H *Phys. Rev. Lett.* **76** 4030 (1996)
75. Fisher L M et al. *Physica C* **403** 219 (2004)
76. Welp U et al. *Phys. Rev. B* **42** 10189 (1990)
77. Welp U et al. *Physica C* **235–240** 241 (1994)
78. Turchinskaya M et al. *Physica C* **221** 62 (1994)
79. Polyanskii A A et al. *Phys. Rev. B* **53** 8687 (1996)
80. Uspenskaya L S, Rakhmanov A L *Phys. Rev. Lett.* **100** 137002 (2008)
81. Uspenskaya L S, Rakhmanov A L *Phys. Rev. B* **79** 144525 (2009)
82. Uspenskaya L S, Kulakov A B, Rakhmanov A L *Phys. Rev. B* **68** 104506 (2003)
83. Uspenskaya L S, Kulakov A B, Rakhmanov A L *Pis'ma Zh. Eksp. Teor. Fiz.* **76** 214 (2002) [*JETP Lett.* **76** 180 (2002)]
84. Dötsch H, Schmitt H J *Appl. Phys. Lett.* **24** 442 (1974)

85. Vlasko-Vlasov V K, Uspenskaya L S *Zh. Eksp. Teor. Fiz.* **91** 1483 (1986) [*Sov. Phys. JETP* **64** 874 (1986)]
86. Uspenskaya L S, Vlasko-Vlasov V K *Zh. Eksp. Teor. Fiz.* **101** 944 (1992) [*Sov. Phys. JETP* **74** 506 (1992)]
87. Dolgopolov V T, Murzin S S *Zh. Eksp. Teor. Fiz.* **73** 2281 (1977) [*Sov. Phys. JETP* **46** 1195 (1977)]
88. Fisher L M et al. *Solid State Commun.* **97** 833 (1996)
89. Fisher L M et al. *Physica C* **278** 169 (1997)
90. Fisher L M et al. *Solid State Commun.* **103** 313 (1997)
91. Mikitik G P, Brandt E H *Phys. Rev. B* **67** 104511 (2003)
92. Indenbom M V et al. *Nature* **385** 702 (1997)
93. D'Anna G et al. *Physica C* **281** 278 (1997)
94. Uspenskaya L S, Korolev K S, Yarykin P N *Physica C* **423** 181 (2005)
95. Uspenskaya L, Korolev K, Kontuganov D *J. Phys. Conf. Ser.* **43** 599 (2006)
96. Uspenskaya L S, Kontuganov D N *Physica C* **460 – 462** 1288 (2007)
97. Landau L D, Lifshitz E M *Phys. Z. Sowjetunion* **8** 153 (1935) [in Landau L D *Sobranie Trudov* (Collected Works) Vol. 1 (Moscow: Nauka, 1969) p. 128]
98. Hubert A *Theorie der Domänenwände in geordneten Medien* (Berlin: Springer-Verlag, 1974) [Translated into Russian (Moscow: Mir, 1977)]
99. Vlasko-Vlasov V K, Khapikov A F *Zh. Tekh. Fiz.* **59** (7) 91 (1989) [*Sov. Phys. Tech. Phys.* **34** 767 (1989)]
100. Kandaurova G S *Usp. Fiz. Nauk* **172** 1165 (2002) [*Phys. Usp.* **45** 1051 (2002)]
101. Kudo K *Phys. Rev. E* **80** 016209 (2009)
102. Dikshtein I E et al. *Zh. Eksp. Teor. Fiz.* **100** 205 (1991) [*Sov. Phys. JETP* **73** 114 (1991)]
103. Dötsch H *J. Magn. Magn. Mater.* **4** 180 (1977)
104. Dötsch H *AIP Conf. Proc.* **29** 78 (1976)
105. Schlömann E *IEEE Trans. Magn.* **11** 1051 (1975)
106. Dedukh L M et al. *Pis'ma Zh. Eksp. Teor. Fiz.* **26** 452 (1977) [*JETP Lett.* **26** 324 (1977)]
107. Gornakov V S et al. *Zh. Eksp. Teor. Fiz.* **82** 2007 (1982) [*Sov. Phys. JETP* **55** 1154 (1982)]
108. Gornakov V S, Dedukh L M, Nikitenko V I *Zh. Eksp. Teor. Fiz.* **86** 1505 (1984) [*Sov. Phys. JETP* **59** 881 (1984)]
109. Vlasko-Vlasov V K, Uspenskaya L S *Zh. Eksp. Teor. Fiz.* **90** 1755 (1986) [*Sov. Phys. JETP* **63** 1029 (1986)]
110. Vlasko-Vlasov V K, Uspenskaya L S *J. Magn. Magn. Mater.* **44** 269 (1984)
111. Vlasko-Vlasov V K, Uspenskaya L S, Khapikov A F *Fiz. Tverd. Tela* **36** 2253 (1994) [*Phys. Solid. State* **36** 1227 (1994)]
112. Vlasko-Vlasov V K et al. *Acta Phys. Pol. A* **68** 53 (1985)
113. Artman J, Charap S, Seagle D *IEEE Trans. Magn.* **19** 1814 (1983)
114. Kandaurova G S, Pashko A G, Osadchenko V Kh *Fiz. Met. Metalloved.* **108** (1) 41 (2009) [*Phys. Met. Metallogr.* **108** 38 (2009)]
115. Hagedorn F B *J. Appl. Phys.* **41** 1161 (1970)
116. Lisovskii F V *Fizika Tsilindricheskikh Magnitnykh Domenov* (Physics of Magnetic Bubbles) (Moscow: Sov. Radio, 1979)